
Research Articles: Behavioral/Cognitive

Visuomotor correlates of conflict expectation in the context of motor decisions

Gerard Derosiere¹, Pierre-Alexandre Klein¹, Sylvie Nozaradan², Alexandre Zénon³, André Mouraux¹ and Julie Duque¹

¹*Institute of Neuroscience, Université catholique de Louvain, Brussels, Belgium*

²*MARC Institute, Western Sydney University, Australia*

³*INCIA, Unité Mixte de Recherche, Centre National de la Recherche Scientifique, Bordeaux, France*

DOI: 10.1523/JNEUROSCI.0623-18.2018

Received: 7 March 2018

Revised: 28 July 2018

Accepted: 1 September 2018

Published: 10 September 2018

Author contributions: G.D., P.-A.K., and S.N. analyzed data; G.D. wrote the first draft of the paper; G.D., S.N., A.Z., A.M., and J.D. edited the paper; G.D. and J.D. wrote the paper; P.-A.K. performed research; S.N., A.Z., A.M., and J.D. designed research.

Conflict of Interest: The authors declare no competing financial interests.

This work was supported by grants from the “Fonds Spéciaux de Recherche” (FSR) of the Université Catholique de Louvain, the Belgian National Funds for Scientific Research (FRS-FNRS: MIS F.4512.14) and the “Fondation Médicale Reine Elisabeth” (FMRE). GD was a postdoctoral fellow supported by a Marie Skłodowska Curie co-fund grant (co-funded by the FNRS). PAK and SN were both PhD students supported by a FNRS grant. AZ was a Senior Research Associate supported by INNOVIRIS.

Corresponding author contact details: Gerard Derosiere, CoActions Lab, Institute of Neuroscience, Université catholique Louvain, Av. Mounier, 53 - Bte B1.53.04, 1200 Bruxelles, Belgium, Tel: + 32 (0)2 764 54 20, Email address: gerard.derosiere@uclouvain.be

Cite as: J. Neurosci ; 10.1523/JNEUROSCI.0623-18.2018

Alerts: Sign up at www.jneurosci.org/cgi/alerts to receive customized email alerts when the fully formatted version of this article is published.

Accepted manuscripts are peer-reviewed but have not been through the copyediting, formatting, or proofreading process.

1 Visuomotor correlates of conflict expectation in the context of motor

2 decisions

⁷ *¹ Institute of Neuroscience, Université catholique de Louvain, Brussels, Belgium*

² MARC Institute, Western Sydney University, Australia

³ INCIA, Unité Mixte de Recherche, Centre National de la Recherche Scientifique, Bordeaux,
France

12 Corresponding author contact details:

13 Gerard Derosiere

14 CoActions Lab

15 Institute of Neuroscience

16 Université catholique Louvain

17 Av. Mounier, 53 - Bte B

18 1200 Bruxelles, Belgium

19 Tel: +32 (0)2 764 54 20

20 Email address: gerard.derosiere@uclouvain.be

21

22 Running title: “Conflict expectation and visuomotor cortex”

23 Number of pages: 50

24 Number of figures: 10

25 Number of tables: 0

26 Number of words: Abstract (250), Introduction (650), Discussion (1609)

27 Conflict of interest: The authors declare no competing financial interests.

Acknowledgements: This work was supported by grants from the “Fonds Spéciaux de Recherche” (FSR) of the Université Catholique de Louvain, the Belgian National Funds for Scientific Research (FRS-FNRS: MIS F.4512.14) and the “Fondation Médicale Reine Elisabeth” (FMRE). GD was a postdoctoral fellow supported by a Marie Skłodowska Curie co-fund grant (co-funded by the FNRS). PAK and SN were both PhD students supported by a FNRS grant. AZ was a Senior Research Associate supported by INNOVIRIS.

34 **ABSTRACT**

35 Many behaviors require choosing between conflicting options competing against each
36 other in visuomotor areas. Such choices can benefit from top-down control processes engaging
37 frontal areas in advance of conflict when it is anticipated. Yet, very little is known about how
38 this proactive control system shapes the visuomotor competition.

39 Here, we used electroencephalography in human subjects (male and female) to identify the
40 visual and motor correlates of conflict expectation in a version of the Eriksen Flanker task that
41 required left or right responses according to the direction of a central target arrow surrounded
42 by congruent or incongruent (conflicting) flankers. Visual conflict was either highly expected
43 (it occurred in 80 % of trials; mostly incongruent blocks [MIBs]) or very unlikely (20% of trials;
44 mostly congruent blocks [MCBs]). We evaluated selective attention in the visual cortex by
45 recording target- and flanker-related steady-state visual-evoked potentials (SSVEPs) and
46 probed action selection by measuring response-locked potentials (RLPs) in the motor cortex.

47 Conflict expectation enhanced accuracy in incongruent trials but this improvement
48 occurred at the cost of speed in congruent trials. Intriguingly, this behavioral adjustment
49 occurred while visuomotor activity was less finely tuned: target-related SSVEPs were smaller
50 while flanker-related SSVEPs were higher in MIBs than in MCBs and incongruent trials were
51 associated with larger RLPs in the ipsilateral (non-selected) motor cortex. Hence, our data
52 suggest that conflict expectation recruits control processes that augment the tolerance for
53 inappropriate visuomotor activations (rather than processes that downregulate their amplitude),
54 allowing for overflow activity to occur without having it turn into the selection of an incorrect
55 response.

56

57

58 **SIGNIFICANT STATEMENT**

59 Motor choices made in front of discordant visual information are more accurate when
60 conflict can be anticipated, probably due to the engagement of top-down control from frontal
61 areas. How this control system modulates activity within visual and motor areas is unknown.
62 Here, we show that when control processes are recruited in anticipation of conflict, as evidenced
63 by higher midfrontal theta activity, visuomotor activity is less finely tuned: visual processing
64 of the goal-relevant location was reduced and the motor cortex displayed more inappropriate
65 activations, compared to when conflict was unlikely. We argue that conflict expectation is
66 associated with an expansion of the distance-to-selection threshold, improving accuracy while
67 the need for online control of visuomotor activity is reduced.

68

69

70

71

72

73

74

75

76

77

78

79

80 **INTRODUCTION**

81 The physical world provides human beings and other animals with a variety of action
82 opportunities, constantly requiring them to make choices. Recent theories posit that motor
83 decisions emerge from a biased competition in a distributed network centered on sensorimotor
84 structures (Derosiere et al., 2015a, 2017a, 2017b; Thura and Cisek, 2014, 2016, 2017).
85 Following this view, a movement is initiated when sensorimotor activity favoring this action
86 reaches a decisive selection threshold (Duque et al., 2017; Klein et al., 2012, 2016; Murphy et
87 al., 2016).

88 The abundance of stimuli in the visual environment makes it often difficult to choose,
89 especially when conflicting sources of information call for incompatible actions (Ardid and
90 Wang, 2013). Imagine for instance a driving scenario in which a traffic light has just turned
91 green and a child suddenly runs across the street. In such circumstances, the inappropriate action
92 (push the accelerator pedal) and the appropriate one (push the brake pedal) are in conflict. At
93 the behavioral level, the presence of conflict induces a cost, reflected by the reduced propensity,
94 and prolonged time needed, to select the correct action (Chen et al., 2009; Mars et al., 2009;
95 Taylor et al., 2007; Töllner et al., 2017). At the neural level, conflict can produce a temporary
96 activation of inappropriate action representations in the motor system (Duque et al., 2016; Klein
97 et al., 2014; Michelet et al., 2010; Szucs et al., 2009; Van Campen et al., 2014; Verleger et al.,
98 2009).

99 In some situations, contextual cues predict the occurrence of conflict (Duque et al., 2016;
100 Stuphorn and Schall, 2006). In the example above, a school sign will help the car driver to
101 anticipate the appearance of children on the street. Accordingly, previous studies have shown
102 that, by increasing conflict expectation, contextual cues help to improve accuracy when
103 conflicting stimuli eventually occur, but tend to slow down responses in easy, non-conflicting
104 trials (Burle et al., 2016; Duque et al., 2016; King et al., 2012; Klein et al., 2014). This

105 behavioral effect is thought to result from enhanced top-down control from frontal areas,
106 including the medial frontal area (Bartoli et al., 2017; Cohen and Ridderinkhof, 2013; Correa
107 et al., 2009; Duque et al., 2013; Spieser et al., 2015; Strack et al., 2013; Vissers et al., 2017),
108 which shows increased electroencephalography (EEG) activity in the theta range (4 to 8 Hz)
109 when conflict is expected (Van Driel et al., 2015). Yet, very little is known about the impact of
110 this control system on the competition occurring in sensorimotor areas during motor decisions.

111 Recently, a study showed that conflict expectation produces a global suppression of
112 corticospinal excitability during motor decisions (Duque et al., 2016; Klein et al., 2014).
113 Notably, this global suppression seems to occur proactively as it is already present at the onset
114 of stimulus occurrence, even before the subjects have eventually perceived the visual cue and
115 its possible conflicting nature. Further, a recent EEG study revealed a more specific suppression
116 of inappropriate motor representations (Burle et al., 2016), but the late occurrence of this effect,
117 merely around the time of movement initiation, questions its role in assisting conflict resolution.
118 Besides, very little is known about the impact of conflict expectation on sensory structures.

119 The goal of the present study was to strengthen our understanding of the sensorimotor
120 changes underlying conflict expectation by considering its impact on action selection in the
121 motor cortex and its effect on selective attention in the visual cortex. More precisely, we
122 investigated whether control processes recruited in anticipation of a visual conflict enhance the
123 selectivity of visual attention and fine-tune action selection. We used EEG to record steady-
124 state visual evoked potentials (SSVEPs) and response-locked potentials (RLPs) while
125 participants performed a modified version of the Eriksen Flanker task (Eriksen and Eriksen,
126 1974) where conflict was either highly expected or unexpected. Finally, we also considered
127 midfrontal theta activity as a marker of cognitive control during conflict expectation (Van Driel
128 et al., 2015).

129

130 **MATERIALS AND METHODS**131 **Participants**

132 20 healthy human subjects participated in the study but 3 of them had to be excluded due
133 to a hardware problem during the experiment. Hence, analyses were run on 17 subjects (9
134 women, 22.3 ± 2.2 years old). All participants were right-handed according to the Edinburgh
135 Questionnaire (Oldfield, 1971) and had normal or corrected-to-normal vision. None of the
136 participants had any neurological disorder, history of psychiatric illness, drug or alcohol abuse,
137 or were under any drug treatment that could influence performance. Participants were
138 financially compensated for their participation. The protocol was approved by the institutional
139 review board of the Université catholique de Louvain, Brussels, Belgium, and required written
140 informed consent.

141

142 **Experimental design**

143 Subjects sat on a comfortable chair in front of a 21-inches cathode ray tube computer
144 screen, with their head supported by a chinrest at 60 cm from the monitor. The display was
145 gamma-corrected and its refresh rate was set at 100 Hz. The left and right forearms were placed
146 on the surface of the table with both hands on the same keyboard positioned upside-down; the
147 left and right index fingers were located on top of the F12 and F5 keys, respectively. Participants
148 wore a 64 Ag/AgCl electrode EEG cap placed according to the international 10/10 system
149 during the whole experiment (Waveguard 64 cap, Cephalon A/S, Denmark). EEG signals were
150 amplified and digitized using a sampling rate of 1000 Hz (64-channel high-speed amplifier,
151 Advanced Neuro Technology, The Netherlands). Electrode impedances were kept below 10
152 kΩ. An average reference was exploited for all recordings. To monitor for artefacts from eye
153 movements, four additional peri-ocular electrodes were placed above and below the left eye

154 (vertical electrooculography; EOG) and at the left and right outer canthi (horizontal EOG).
155 Finally, an Eyelink© 1000 + eye tracker (SR Research Ltd., Kanata, Ontario, Canada; RRID:
156 SCR_009602) was used to monitor the subjects' gaze during the experiment (sampling rate:
157 500 Hz). Subjects were required to maintain their gaze on the fixation point during each trial
158 (see *Task* section, below). When deviations occurred, subjects were asked to correct their gaze
159 position. Trials with gaze deviation were excluded from the analyses.

160

161 **Task**

162 We used a modified version of the Eriksen Flanker Task (Eriksen & Eriksen 1974; see
163 Klein et al., 2014; Duque et al., 2016). The task was implemented by means of Matlab 6.5 (The
164 Mathworks, Natick, Massachusetts, USA, RRID: SCR_001622) and the Cogent 2000 toolbox
165 (Functional Imaging Laboratory, Laboratory of Neurobiology and Institute of Cognitive
166 Neuroscience at the Wellcome Department of Imaging Neuroscience, London, UK; RRID:
167 SCR_015672). Subjects were required to perform a left or right index finger keypress according
168 to the orientation of a left or right-pointing arrow (*i.e.*, < or >, respectively). This “target” was
169 surrounded by a set of two irrelevant arrows on each side, referred to as “flankers”, which either
170 pointed in the same direction (congruent stimuli, “<<<<” or “>>>>”) or in the opposite
171 direction (incongruent stimuli, “>><>>” or “<<>><>”; dimensions of the arrows: 18 × 18 mm;
172 arrows were located at 2 mm from each other; whole stimulus length: 98 mm). Hence,
173 imperative stimuli were either congruent or incongruent, and instructed either left or right index
174 finger key-presses (four trial types; see Figure 1.A).

175 Each trial started with the onset of five horizontally aligned black squares (*i.e.*, 18 × 18
176 mm, located at 2 mm from each other; stimulus length: 98 mm) appearing 15 mm above a
177 central point (Figure 1.B; see “SSVEP procedure” section below for an explanation regarding
178 the slight lateralization of the squares with respect to the central point). Subjects were asked to

179 keep fixation on the central point during the whole trial. After 7000 ms, the squares were
180 replaced by the imperative stimulus which consisted of one of the four possible combinations
181 of target and flankers described above (“<<<<”, “>>>>”, “>><>>” or “<><><”). The
182 target always appeared at the location of the central square whereas the flankers occurred at the
183 other square locations. In some trials (6% of total number of trials; that is, 24 trials), the
184 imperative stimulus appeared earlier than expected (between 1000 ms and 6500 ms instead of
185 7000 ms). Such “catch” trials were included to make sure that the subjects were focused on the
186 task from the beginning of each trial and ready to react as soon as the imperative stimulus
187 appeared; these trials were not taken into account for the data analysis. Subjects were required
188 to respond as quickly as possible following the imperative stimulus. A mask appeared once the
189 subject had answered (or after 700 ms). The latter consisted of five aligned and overlapping
190 double-arrows (see Figure 1.B) which remained on the screen for an interval of 1200 ms. A
191 feedback was then presented for 1500 ms. This feedback consisted of a positive score depicted
192 in green (following a correct response) or a negative score depicted in red (following an
193 incorrect response). Positive scores were always inversely proportional to the RTs; the faster
194 the response, the higher the score (score = k/RT with $k = 5000$). For instance, a correct response
195 provided with a RT of 400 ms yielded a score of +12.5 points. Incorrect responses were always
196 followed by a fixed negative score (-10). The total amount of points accumulated from the
197 beginning of each block was also presented following each trial, just below the current trial
198 score. Subjects knew they would receive a financial bonus depending on their final score.

199

200 **Experimental blocks**

201 All subjects came for one session of eight experimental blocks. Each block comprised the
202 same percentage of left and right finger responses (50% left / 50% right). In contrast, the
203 percentage of congruent and incongruent trials varied in two different block types (Figure 1.C).

204 In a first type of block, called “mostly congruent block” (MCB), most trials were congruent
205 (80%) and very few were incongruent (20%). In contrast, the second block type, called “mostly
206 incongruent block” (MIB), involved a majority of incongruent trials (80%) and few congruent
207 ones (20%). Subjects were always told about the type of block (MCB or MIB) they would be
208 performing next. Hence, the degree to which subjects expected conflict clearly differed between
209 the two block types (Duque et al., 2016; Klein et al., 2014; Ridderinkhof, 2002). Conflict
210 expectation was high in the MIBs, because subjects knew they would have to face incongruent
211 flankers on most trials, whereas it was low in the MCBs, given the rarity of incongruent flankers
212 in the latter blocks.

213 At the beginning of the session, subjects performed two blocks of forty trials in a neutral
214 condition (same amount of congruent and incongruent trials). This allowed them to become
215 familiar with the two trial types. Subjects then performed the eight experimental blocks (*i.e.*,
216 four MCBs and four MIBs), each of which consisted of forty trials. The same block types were
217 run in a row but their order was counterbalanced between subjects. Each block lasted around 7
218 minutes and the whole experiment duration was about 90 minutes.

219

220 **SSVEP procedure**

221 The five squares presented before the imperative signal were used to obtain SSVEPs in
222 both contexts (MCB and MIB). The position of these squares varied on the horizontal meridian
223 in two different block types (Figure 1.D). In half of the blocks, the five squares were slightly
224 shifted to the left (referred to as “left-shifted” stimuli) whereas they were slightly shifted to the
225 right in the other blocks (“right-shifted” stimuli; 10 mm of eccentricity). As a result, the central
226 “target square” (Targets_q) either appeared on the left or on the right side of the central fixation
227 point (*i.e.*, on the right in right-shifted trials or on the left in left-shifted trials). This variation
228 in the stimulus position was set to reduce any putative effect of habituation on SSVEP measures

229 due to the repetition of the stimulation at a given screen location (Moratti et al., 2007; Kus et
230 al., 2013). Left- and right-shifted stimuli were grouped in separate blocks ordered in a
231 counterbalanced way.

232 The squares were flickering at one of three different frequencies to induce three separate
233 location-specific SSVEPs (flickering elicited by a contrast of luminance; Norcia et al., 2015;
234 Vialatte et al., 2010, McTeague et al., 2015; Figure 1.D). One frequency (16.6 Hz) was
235 selectively used to tag the Targets_{sq}. Another frequency (12.5 Hz) was used to tag the most
236 central (C) “flanker square” that was located on the other side of the fixation point (Flanker-
237 Cs_q; see below). A third frequency (14.2 Hz) was used for the three other flanker squares, which
238 were more peripheral (P) with respect to the fixation point (Flanker-Ps_q). The flickering stopped
239 when the arrow stimulus occurred (*i.e.*, at the end of the fixation period).

240 Previous studies have shown that flickering stimuli presented in one visual hemifield elicit
241 a predominant SSVEP response in the contralateral hemisphere and an attenuated response in
242 the ipsilateral hemisphere (*e.g.*, Kim et al., 2008, 2011). Therefore, we expected the Targets_{sq}
243 and Flanker-Cs_q to elicit predominant SSVEP responses in opposite hemispheres (given that
244 they are located on opposite sides of the fixation point). For instance, in left-shifted trials, we
245 expected the Targets_{sq} and Flanker-Cs_q to elicit predominant SSVEP responses in the right and
246 left hemispheres, respectively, whereas the reversed pattern was expected in right-shifted trials,
247 as confirmed by our analyses (see Results section). Conversely, we predicted that the three
248 Flanker-Ps_q would elicit comparable SSVEP responses in both hemispheres as these squares
249 were shared out on both sides of the central fixation point. Moreover, based on previous studies,
250 we expected the SSVEP responses to be most prominent in the signal recorded at occipito-
251 parietal electrodes, capturing responses originating mostly in the underlying visual cortex,
252 though parietal and frontal sources are not excluded (Di Russo et al., 2007; Gulbinaite et al.,
253 2017; Heinrichs-Graham and Wilson, 2012; Kim et al., 2011).

254 The amplitude of SSVEPs is known to reflect how much visuospatial attention is allocated
255 to the flickering stimuli, regardless of whether attention is overtly or covertly oriented towards
256 them (Keil et al., 2006; Müller et al., 2006; Norcia et al., 2015; Shioiri et al., 2016; Vialatte et
257 al., 2010). In the present study, we compared SSVEPs in MIBs and MCBs to investigate the
258 influence of conflict expectation on the allocation of covert attention towards goal-relevant
259 ($\text{Targets}_{\text{q}}$) and goal-irrelevant (Flanker-C_{Sq} and Flanker-P_{Sq}) stimulus locations.

260

261

262 *****

263 *Figure 1 about here*

264 *****

265

266

267 **Behavioral measurements**

268 *Data analysis*

269 Finger responses were classified according to the responding hand (*i.e.*, left or right hand),
270 the trial type (*i.e.*, congruent or incongruent trial) and the context (*i.e.*, MCB or MIB). For each
271 of these conditions, we calculated the percentage of correct responses (accuracy) and their
272 reaction time (RT). Accuracy and RT data were log-transformed for the statistical analyses in
273 order to normalize their distribution.

274

275 *Statistical analysis*

276 Statistica software (version 7.0, Statsoft, Oklahoma, United-States, RRID: SCR_014213)
277 was used for the analysis of the accuracy and RT data. All data were examined for normality
278 and homogeneity of variance using Skewness, Kurtosis and Brown-Forsythe tests. RT and
279 accuracy were analyzed separately using two three-way repeated-measure analyses of variance
280 (ANOVA) with HAND (left, right), TRIAL (congruent, incongruent), and CONTEXT (MCB,
281 MIB) as within-subject factors. When appropriate, Fisher's LSD post-hoc tests were used to
282 detect paired differences. The significance level was set at $p < .05$. Results are expressed as
283 mean \pm standard error (SE).

284

285 **Visuomotor activity**

286 *Data analysis*

287 All EEG data were processed on Matlab (The Mathworks Inc. Natick, Massachusetts,
288 USA) using Letswave 6 (Mouraux and Iannetti, 2008) and EEGLAB (RRID: SCR_007292;
289 Delorme and Makeig, 2004). The EEG signals were filtered using a 0.01 to 70 Hz bandpass
290 butterworth filter; they were then segmented in two subsets.

291 The first subset was comprised of epochs extending from +1000 to +7000 ms with respect
292 to the onset of the 5-square stimulus. These epochs were used to extract the SSVEPs and thus
293 served to evaluate the distribution of visual attention in space (*i.e.*, attention epochs) according
294 to the degree of conflict expectation (larger in MIBs than in MCBs). We discarded the first
295 1000 ms of the flickering period to avoid contamination from the initial event-related brain
296 potential (ERP) on the SSVEP as well as to ensure sensitivity to conditioning effects typically
297 occurring later in the epoch (Moratti et al., 2006; Keil et al., 2013).

298 The second subset was comprised of epochs extending from -700 to -50 ms with respect to
299 the onset of the key-press. These epochs were used to extract the RLPs and thus served to

300 characterize the motor correlates of action selection (*i.e.*, selection epochs) according to the
301 level of conflict (larger in incongruent than in congruent trials) and the degree of conflict
302 expectation (larger in MIBs than in MCBs). We also considered the influence of responding
303 with the right (dominant) or left (non-dominant) hand.

304 For both subsets of epochs, an Independent Component Analysis (ICA) was computed to
305 remove components corresponding to eye blinks and electrical line noise (Delorme et al., 2007);
306 the data were then screened visually and epochs with residual artifacts were rejected.

307

308 SSVEP data

309 SSVEPs were obtained to evaluate visual cortical correlates of selective attention. To do
310 so, attention epochs were first classified according to the stimulus shift (left- or right-shifted)
311 and the context in which they were recorded (MCB, MIB). Following this classification, a total
312 of 78 ± 4 epochs were obtained per condition. Each epoch was then sectioned in two sub-epochs
313 of 3000 ms duration: the first sub-epoch extended from +1000 to +4000 ms and served to assess
314 selective attention at an early stage of the fixation period (Stage_{Early}) while the second one,
315 extending from +4000 to +7000 ms, served to assess attention at a later stage of fixation
316 (Stage_{Late}). For each condition obtained (*i.e.*, Stage_{Early}/Stage_{Late}, left-/right-shifted, MCB/MIB),
317 the epochs were averaged to attenuate the contribution of neural activity that was not phase-
318 locked to the onset of the square stimulus (Derosiere et al., 2015b). A current source density
319 (CSD) transformation was applied to the scalp voltage data to enhance the spatial specificity of
320 the signals (Burle et al., 2015; McTeague et al., 2015; Vidal et al., 2015).

321 The signals were zero-padded with 2000 points in order to increase the frequency
322 resolution of the ensuing Fast-Fourier Transform (FFT) analysis (Chabuda et al., 2018; Diez et
323 al., 2011; Gruss et al., 2012). For each sub-epoch, the number of points was thus extended from

324 3000 points (*i.e.*, epochs of 3000 ms sampled at 1000 Hz; see above) to 5000 points. A discrete
325 FFT was then applied to convert the signals in the frequency domain (Frigo and Johnson, 1998),
326 yielding spectra from 0.1 to 500 Hz with a resolution of 0.2 Hz (Bach and Meigen, 1999).
327 Background noise was removed by computing, for each point of the spectra, its z-score value
328 with respect to the values measured at neighboring frequency bins (2th to 5th frequency bins
329 relative to each bin; Mouraux et al., 2011; Nozaradan et al., 2011, 2012, 2017; Rossion et al.,
330 2012).

331 Based on the scalp topographies and on the literature, we defined an occipito-parietal
332 region of interest (ROI) for which SSVEP amplitudes are known to be maximal when elicited
333 by a contrast of luminance (McTeague et al., 2015; Rossion et al., 2012). This posterior ROI
334 (ROI_{Post}) included the O1, O2, PO3, PO4, P3, P4, P5, P6, P7 and P8 electrodes (Figure 2.A).
335 Half of these electrodes are located over the left hemisphere (O1, PO3, P3, P5 and P7), whereas
336 the other half are over the right hemisphere (O2, PO4, P4, P6 and P8). To assess SSVEPs
337 emerging in the hemisphere contralateral to the Targets_q (HEMI_{Contra-to-Target}), we pooled
338 together the data from corresponding electrodes in both hemispheres (*e.g.*, O1 and O2) collected
339 during left- and right-shifted trials. That is, SSVEPs recorded from O2, PO4, P4, P6 and P8
340 (right-sided electrodes) during left-shifted trials were pooled with those obtained at O1, PO3,
341 P3, P5 and P7 (left-sided electrodes) during right-shifted trials, respectively. The resulting
342 “pooled” scalp locations in the HEMI_{Contra-to-Target} are referred to by numbers from 1 to 5
343 according to the location of each pair of original electrodes, beginning with the most caudo-
344 medial ones (ROI_{Post_1} = O1 and O2) and ending with the most rostro-lateral ones (ROI_{Post_5} =
345 P7 and P8; see Figure 2.A). Likewise, to evaluate SSVEPs emerging in the hemisphere
346 ipsilateral to the Targets_q (HEMI_{Ipsi-to-Target}), we pooled together the data recorded from O2,
347 PO4, P4, P6 and P8 (right-sided electrodes) during right-shifted trials and the data recorded
348 from O1, PO3, P3, P5 and P7 (left-sided electrodes) during left-shifted trials, respectively. The

349 resulting “pooled” scalp locations in the HEMI_{Ipsi-to-Target} are also referred to as ROI_{Post_1-5}. Note
350 that because the Targets_q and Flanker-C_{Sq} were always located on opposite sides of the fixation
351 point, the hemisphere contralateral to the Flanker-C_{Sq} was the HEMI_{Ipsi-to-Target}, whereas the one
352 ipsilateral to the Flanker-C_{Sq} was the HEMI_{Contra-to-Target}.

353 Frequency spectra extracted from the ROI_{Post_1} to ROI_{Post_5} electrodes were exploited to
354 compute linear channel maps. In Figure 2.A, the electrodes were disposed along the y-axis
355 according to their scalp location (from ROI_{Post_1} to ROI_{Post_5}) and the spectral amplitude
356 obtained at each frequency (x-axis) was linearly interpolated (see Langer et al., 2017, for a
357 similar approach). In each subject, eight maps were obtained. That is, we obtained a map for
358 each hemisphere (HEMI_{Contra-to-Target}, HEMI_{Ipsi-to-Target}), each context (MCB, MIB) and each
359 stage of the fixation period (Stage_{Early}, Stage_{Late}).

360

361 RLP data

362 RLPs were obtained to evaluate motor cortical correlates of action selection. To do so,
363 selection epochs were classified according to the responding hand (left, right), the trial type
364 (congruent, incongruent) and the context in which they were recorded (MCB, MIB). Epochs
365 obtained from trials where an incorrect response was provided were discarded from further
366 analysis. Following this classification, a total of 35 ± 6 epochs were obtained per condition. For
367 each condition, the epochs were averaged to attenuate the contribution of neural activity that
368 was not phase-locked to the onset of the key press (Derouiere et al., 2015b) and a baseline
369 subtraction was applied (time window for baseline correction: -700 to -500 ms). The signals
370 were subsequently cropped at -500 ms and CSD transformation was applied to the scalp voltage
371 data to enhance the spatial specificity of the signals (Burle et al., 2015; McTeague et al., 2015;
372 Vidal et al., 2015).

373 Based on the obtained scalp topographies and on the literature, we defined a central ROI
374 ($ROI_{Central}$) for which the RLP amplitudes are maximal close to movement execution (Cottereau
375 et al., 2014; Clark et al., 2015). The central ROI included the C1, C2, C3, C4, C6, C7, T7 and
376 T8 electrodes (Figure 2.B). Half of these electrodes are located over the left hemisphere (C1,
377 C3, C7 and T7), whereas the other half are over the right hemisphere (C2, C4, C6 and T8). To
378 assess RLPs emerging in the hemisphere contralateral to the responding hand ($HEMI_{Contra-to-}$
379 $Resp$), we pooled together the data from corresponding electrodes in both hemispheres (e.g., C4
380 and C3) collected in trials in which subjects provided left and right hand responses. That is, the
381 RLPs recorded from C2, C4, C6 and T8 (right-sided electrodes) when subjects provided left
382 hand responses were pooled with those obtained at C1, C3, C7 and T7 (left-sided electrodes)
383 when they responded with the right hand, respectively. The resulting “pooled” scalp locations
384 in the $HEMI_{Contra-to-}Resp$ are referred to by numbers from 1 to 4 according to the location of each
385 pair of original electrodes, beginning with the most medial ones ($ROI_{Central_1} = C1$ and $C2$) and
386 ending with the most lateral ones ($ROI_{Central_4} = T7$ and $T8$). Likewise, to evaluate the RLPs
387 emerging in the hemisphere ipsilateral to the responding hand ($HEMI_{Ipsi-to-}Resp$), we pooled
388 together the data recorded from C2, C4, C6 and T8 (right-sided electrodes) when subjects
389 provided a right hand response and the data recorded from C1, C3, C7 and T7 (left-sided
390 electrodes) when they responded with the left hand, respectively. Again, these “pooled” scalp
391 locations in the $HEMI_{Ipsi-to-}Resp$ are referred to as $ROI_{Central_1-4}$.

392 RLPs extracted from $ROI_{Central_1}$ to $ROI_{Central_4}$ electrodes were exploited to compute linear
393 channel maps. In Figure 2.B, the electrodes were disposed along the y-axis according to their
394 scalp location (from $ROI_{Central_1}$ to $ROI_{Central_4}$) and the amplitude of the RLP obtained at each
395 time point (x-axis) was linearly interpolated. In each subject, sixteen maps were obtained. That
396 is, we obtained a map for each hemisphere ($HEMI_{Contra-to-}Resp$, $HEMI_{Ipsi-to-}Resp$), for each hand

397 response (left, right), in the two trial types (congruent, incongruent) and in both contexts (MCB,
398 MIB).

399

400 *Statistical analysis*

401 The SSVEP and RLP maps were analyzed using a cluster-based statistical method
402 (Bullmore et al., 1999; Maris, 2012; Maris and Oostenveld, 2007; Poline and Mazoyer, 1993).
403 This approach allows to run analyses on multiple data points while accounting for both the
404 multiplicity of the statistical tests realized and the spatial dependency between the points. It was
405 initially developed for the statistical analysis of structural magnetic resonance imaging (MRI)
406 data (Bullmore et al., 1999; Poline and Mazoyer, 1993) and has been then extended to EEG
407 work (Maris and Oostenveld, 2007), where it has been widely used ever since (*e.g.*, Craddock
408 et al., 2017; Frehlich et al., 2016; Groppe et al., 2011; Melloni et al., 2015; Pernet et al., 2015).

409 Here, we used a cluster-based analysis of SSVEP maps to assess the effect of the factors
410 HEMISPHERE (HEMI_{Contra-to-Target}, HEMI_{Ipsi-to-Target}), CONTEXT (MCB, MIB) and TIME
411 (Early, Late). Besides, the cluster-based analysis of RLP maps included the factors
412 HEMISPHERE (HEMI_{Contra-to-Resp}, HEMI_{Ipsi-to-Resp}), HAND (left, right), TRIAL (congruent,
413 incongruent) and CONTEXT (MCB, MIB). Note that the factor TRIAL was not included in the
414 analysis of the SSVEPs as the imperative arrows (determining the trial type) only appeared after
415 the flickering period.

416 Concretely, in a first step, a point-by-point ANOVA is performed using the factors
417 mentioned above, hence yielding F- and p-values for each data point. Points with an F-value
418 exceeding an alpha level of $p = .05$ are selected. Among the selected points, those that are
419 located next to each other on the map are grouped together in clusters. For each cluster so

420 obtained, cluster-level F-values are subsequently computed by adding up the F-value associated
421 with each individual data point comprised in the cluster.

422 Then, in a second step, Monte-Carlo permutation tests are performed. For each subject,
423 maps are randomly permuted, resulting in a so-called "random partition" (separate analyses on
424 SSVEP and RLP maps). This step can be considered as equivalent to randomly switching the
425 labels of the maps, independently for each subject. Based on the random partition, a point-by-
426 point ANOVA is performed in the exact same manner as during step 1 and cluster-level F-
427 values are computed. The random partitioning and the subsequent calculation of the cluster-
428 level F-values are re-iterated 1000 times. A histogram of the F-values is then constructed. For
429 each factor and interaction tested, the proportion of random partitions that results in larger F-
430 values than the one observed in the first step of the analysis is finally calculated. This proportion
431 represents the Monte-Carlo significance probability, also called p-value. If, for a given effect
432 and a given point, less than 5 % of the random partitions results in a larger F-value than the one
433 observed in the first step of the analysis, then it is considered as significant for that cluster at p
434 < .05.

435 For each factor and interaction, the analysis outputs a map highlighting the cluster(s) that
436 survived to the thresholding at the Monte-Carlo significance probability. Based on these maps,
437 the onset and offset of the cluster(s) can be estimated. Note however that the onset and offset
438 of where each cluster exceeds the threshold depends on several factors including the frequency
439 / temporal resolution of the SSVEP / RLP maps. Hence, when referring to the cluster edges in
440 the followings, one should be aware that they could have slightly varied if different parameters
441 had been exploited during data processing.

442 Importantly, combining a cluster-based approach with Monte-Carlo permutations allowed
443 us to identify the data points, within the SSVEP and RLP maps, showing a significant effect of
444 the factors mentioned above in a data-driven way (*i.e.*, by testing all the points of the maps).

445 Such a data-driven approach prevented us from arbitrarily selecting a number of frequency or
446 temporal bins from the continuous signals of the SSVEP and RLP maps, respectively, and from
447 a priori averaging the signals across the ROI_{Post} or ROI_{Central} electrodes, as both procedures
448 could have impacted the statistical results (Cohen and Gulbinaite, 2017; Pernet et al., 2015;
449 Shen et al., 2017).

450 When a significant effect involved more than two conditions, post-hoc tests were required
451 to test which pairwise difference(s) drove the statistical difference detected. For each condition,
452 the values of every data point composing the detected cluster were averaged into a single value;
453 Fisher LSD post-hoc tests were used to detect paired differences on the averaged values. The
454 significance level was set at $p < .05$. Results are expressed as mean \pm standard error (SE).

455

456 *****

457 *Figure 2 about here*

458 *****

459

460 **Midfrontal theta activity**

461 *Data analysis*

462 Conflict expectation has been shown to increase midfrontal theta activity (*i.e.*, [4 - 8 Hz];
463 Van Driel et al., 2015), a well-known substrate of cognitive control (*e.g.*, Gulbinaite et al.,
464 2014; Lin et al., 2018; Vissers et al., 2018; Wang et al., 2017). While the primary aim of the
465 present study was to investigate the impact of conflict expectation on visuomotor activity, we
466 also tested whether the effect reported on midfrontal theta activity could be replicated based on
467 our dataset. To do so, we exploited the same time-frequency (TF) analysis as in Van Driel et al.

468 (2015) and applied it on the EEG signals obtained during the fixation period (same epoch as for
469 the SSVEPs).

470 First, attention epochs (*i.e.*, as defined in the SSVEP section) were classified according to
471 the context in which they were recorded (MCB, MIB). Second, EEG signals were decomposed
472 into their TF representations for both contexts, every electrode and each subject. TF maps were
473 obtained by multiplying them with a series of Morlet wavelets with frequencies ranging from 4
474 to 9 Hz in 20 linearly scaled steps. The wavelets were generated by multiplying perfect sine
475 waves (sine wave = $e^{i2\pi ft}$, where i is the complex operator, f is the frequency, and t is time) with
476 a Gaussian (Gaussian = $e^{-t^2/2\sigma^2}$, where σ is the width of the Gaussian). The width of the Gaussian
477 was set to four cycles [$\sigma = 4/(2\pi f)$], in order to trade-off temporal and frequency resolution. The
478 FFT was applied to both the EEG signals and the Morlet wavelets, and these were then
479 multiplied in the frequency domain, after which the inverse FFT was applied. From the resulting
480 complex signal Z_t , an estimate of frequency-specific amplitude at each time point was defined
481 as $[\text{real}(Z_t)^2 + \text{imag}(Z_t)^2]$. Third, trials were averaged together, resulting in one TF map per
482 condition, per electrode and per subject. Finally, in order to make the data comparable across
483 all frequencies and subjects, difference maps were computed by subtracting the spectral
484 amplitude (SpectAmp) obtained at each TF point in the MCB condition from the corresponding
485 values in the MIB condition (Castro et al., 2018). Hence, this analysis yielded one TF map per
486 electrode and per subject, on which the difference in spectral amplitude between MIBs and
487 MCBs was represented (Δ SpectAmp). Δ SpectAmp values higher than 0 denoted a higher
488 spectral power in MIBs compared to MCBs.

489

490 *Statistical analysis*

491 The statistical analysis was realized on the TF map obtained at the Fz electrode, for which
492 the effect of conflict expectation on theta activity is the strongest (Van Driel et al., 2015, see

493 also Herz et al., 2017). A cluster-based analysis was performed in the exact same way as
494 described above on this TF map, except that we used a two-way Student's t-test against 0 (*i.e.*,
495 instead of an ANOVA). The aim of this analysis was to detect the cluster(s) of data points on
496 the TF map for which Δ SpectAmp values were higher than 0 at the Monte-Carlo significance
497 probability of .05.

498

499 **RESULTS**

500 **Behavior**

501 *Accuracy*

502 The ANOVA performed on the accuracy data revealed a tendency towards a significant
503 effect of the factor HAND ($F_{1,16} = 4.13$, $p = .059$). In fact, the percentage of correct responses
504 tended to be lower when the imperative stimulus required a left than a right hand movement
505 (84.78 ± 2.48 and 91.47 ± 1.09 % of correct responses, respectively; both trial types and
506 contexts pooled together; log-transformed data are represented on Figure 3.A). Hence, subjects
507 tended to be less accurate when they had to respond with the non-dominant hand compared to
508 when they had to answer with the dominant one. In other words, they were more prone to
509 respond with the dominant hand even when the target arrow instructed them to make the
510 opposite choice.

511 The ANOVA also revealed a significant main effect of the factor TRIAL on the accuracy
512 data ($F_{1,16} = 16.56$, $p = .0008$). The percentage of correct responses was lower in incongruent
513 (79.59 ± 2.72 %) than in congruent trials (96.67 ± 0.97 %, both hands and contexts pooled
514 together; Figure 3.B). Hence, as expected, subjects made more errors when the flankers pointed
515 to the incorrect response compared to when they pointed to the correct one.

516 Importantly, the TRIAL effect reported above depended on the CONTEXT within which
517 the responses were provided (MCB or MIB), as revealed by a significant TRIAL*CONTEXT
518 interaction ($F_{1,16} = 22.82$, $p = .0002$). In fact, the difference in accuracy between congruent and
519 incongruent trials was attenuated in the MIBs compared to the MCBs. That is, subjects made
520 much less errors in the presence of incongruent flankers when the latter had been anticipated
521 (in MIBs, 85.06 ± 2.68 % of correct responses) compared to when incongruent flankers were
522 unlikely (MCBs, 74.11 ± 3.31 %, $p < .00001$; both hands pooled together; Figure 3.C). Hence,
523 control processes associated with conflict expectation helped subjects to reduce the negative
524 impact of incongruent information on their decision accuracy, as previously shown (Burle et
525 al., 2016; Duque et al., 2016; King et al., 2012; Klein et al., 2014). Notably, congruent trials
526 were associated with a comparable accuracy in MIBs (95.65 ± 1.74 %) and MCBs ($97.68 \pm$
527 0.63 %; $p = .426$).

528

529 *Reaction time*

530 The ANOVA revealed a significant main effect of the factor HAND on the RT data ($F_{1,16}$
531 $= 11.45$, $p = .004$), with longer response times for left (500 ± 12 ms) than right hand movements
532 (482 ± 11 ms; both trial types and contexts pooled together; log-transformed in Figure 3.D).
533 Hence, it took more time for the subjects to respond when the target indicated a non-dominant
534 hand response compared to when a movement with the dominant hand was required. These
535 findings are in agreement with the accuracy data indicating a preference for responding with
536 the dominant hand.

537 As expected, the ANOVA also showed a significant main effect of the factor TRIAL ($F_{1,16}$
538 $= 91.06$, $p < .00001$); RTs were longer in incongruent (548 ± 17 ms) than in congruent trials
539 (435 ± 7 ms, both hand and contexts pooled together; Figure 3.E). Interestingly, this TRIAL
540 effect also depended on the CONTEXT within which the responses were provided, as revealed

541 by a significant TRIAL*CONTEXT interaction on the RT data ($F_{1,16} = 11.52$, $p = .003$). As
542 depicted in Figure 3.F, the RT difference between congruent and incongruent trials was
543 attenuated in MIBs compared to MCBs. Interestingly, this effect was not due to a fastening of
544 response times on incongruent trials; the latter trials were associated with comparable RTs in
545 MIBs (544 ± 19 ms) and MCBs (551 ± 18 ms; $p = .209$). In contrast, RTs on congruent trials
546 varied between the two block types; they were significantly longer in MIBs (445 ± 8 ms)
547 compared to MCBs (424 ± 8 ms; $p = .003$). Hence, control processes associated with conflict
548 expectation did not allow subjects to respond faster. On the contrary, they tended to slow down
549 RTs following congruent signals.

550 Notably, the scores provided at the end of each trial tended to be higher in MIBs (average
551 score: 8.50 ± 0.46 a.u) than in MCBs (average score: 7.79 ± 0.40 a.u.), consistent with the
552 higher accuracy in the former block types. However, this effect was not significant. ; $t_{1,16} = -$
553 1.839 ; $p = .084$). This negative finding may be explained by the fact that the scores not only
554 depended on the accuracy (which showed a main effect of BLOCK; $F_{1,16} = 7.33$, $p = .01$) but
555 also relied on the reaction time (which was comparable in both BLOCK types; $F_{1,16} = 1.15$, $p =$
556 $.30$). Hence, overall, the feedback was roughly comparable in MCBs and in MIBs.

557 In conclusion, the behavioral data indicate that conflict expectation is associated with the
558 recruitment of control processes that enhance the ability to solve conflicting visuomotor
559 choices. However, this amelioration occurs at the cost of speed: subjects become more accurate
560 on incongruent trials but respond more slowly to easy, congruent signals.

561

562 *****

563 *Figure 3 about here*

564 *****

565

566

567 **Midfrontal theta activity**

568 The cluster-based statistical analysis revealed that Δ SpectAmp was significantly different
569 from 0 for a cluster of data points (*i.e.*, cluster thresholded at the Monte-Carlo significance
570 probability of .05; Figure 4.A). The cluster extended from +4700 to +5400 ms and from 6 to 8
571 Hz, hence largely overlapping with the theta range (*i.e.*, [4 – 8 Hz]). Visual inspection of the
572 grand-average TF map obtained for the Fz electrode (Figure 4.B) indicates that the Δ SpectAmp
573 was positive in this TF window, revealing a higher spectral amplitude in MIBs than in MCBs.
574 Further, visual inspection of the topography (Figure 4.C) suggests that this effect is restricted
575 to the Fz electrode: Δ SpectAmp was higher at Fz than at any other midline electrodes. To
576 provide statistical evidence for this observation, the values of each data point composing the
577 cluster were averaged into a single value for the Fz, the Fpz (anterior to Fz), and the Cz
578 (posterior to Fz) electrodes. An ANOVA performed on these average Δ SpectAmp values
579 revealed a significant effect of the factor ELECTRODE ($F_{2,30} = 5.58$, $p = .008$); Fisher LSD
580 post-hoc tests showed that Δ SpectAmp was indeed significantly higher at Fz (140.88 ± 25.63
581 $\mu\text{V}/\text{m}^2$) than at both Fpz ($-36.56 \pm 58.41 \mu\text{V}/\text{m}^2$; $p = .006$) and Cz ($-33.08 \pm 36.47 \mu\text{V}/\text{m}^2$; $p =$
582 .007), with no significant difference between Fpz and Cz ($p = .954$; Figure 4.D). Hence,
583 consistent with previous findings in the literature (Van Driel et al., 2015), conflict expectation
584 increased midfrontal theta activity in the present study, corroborating the idea that it represents
585 an important marker of cognitive control (Gulbinnaite et al., 2014; Herz et al., 2017; Lin et al.,
586 2018; Vissers et al., 2018; Wang et al., 2017).

587

588 *****

589

Figure 4 about here

590

591

592 **Visuomotor activity**593 *SSVEP data*

594 The cluster-based statistical analysis revealed a significant main effect of the factor
595 HEMISPHERE on two clusters of data points (cluster thresholded at the significance
596 probability of .05; Figure 5.A). A first cluster was centered on the Targets_q frequency ([16.4 Hz
597 - 16.8 Hz]) and spread over the five ROI_{Post_1-5} locations (Figure 5.C). As expected, the SSVEP
598 amplitude was higher in this frequency range for the HEMI_{Contra-to-Target} than for the HEMI_{Ipsi-to-}
599 Target ($p < .0001$). A second cluster was centered on the Flanker-C_{Sq} frequency ([12.3 Hz - 12.7
600 Hz]) and extended from ROI_{Post_2} to ROI_{Post_5}. Here, the SSVEP amplitude was lower for the
601 HEMI_{Contra-to-Target} than for the HEMI_{Ipsi-to-Target} ($p = .0009$; Figure 5.B). This was expected given
602 that the two hemispheres are, respectively, ipsilateral and contralateral to the Flanker-C_{Sq} (see
603 Method section). Hence, both the Targets_q and the Flanker-C_{Sq} elicited predominant SSVEP
604 responses in the contralateral hemisphere. Such an effect of HEMISPHERE was not observed
605 for the Flanker-P_{Sq} frequency (*i.e.*, at 14.2 Hz), consistent with the fact that these squares were
606 located on both sides of the central fixation point.

607

608

609

Figure 5 about here

610

611

612 Interestingly, the cluster-based analysis also showed a significant main effect of the factor
613 CONTEXT (cluster thresholded at the significance probability of .05; Figure 6.A). The cluster
614 was centered on the Flanker-Psq frequency ([14.0 Hz - 14.4 Hz]) and expanded from ROI_{Post_1}
615 to ROI_{Post_3} (Figure 6.B). In this cluster, SSVEP amplitude was lower in MCBs than in MIBs
616 ($p = .013$), suggesting a surprisingly higher attention toward goal-irrelevant locations when
617 conflict was expected compared to when it was unlikely.

618

619 *****

620 *Figure 6 about here*

621 *****

622

623 Finally, the cluster-based analysis revealed a significant effect of the factor TIME on a
624 cluster centered on the Targets_q frequency ([16.4 Hz - 16.8 Hz]) and expanding from ROI_{Post_2}
625 to ROI_{Post_5} (cluster thresholded at the significance probability of .05); here, the SSVEP
626 amplitude appeared to be higher at Stage_{Late} than at Stage_{Early} ($p < .0001$). However, this effect
627 of TIME depended on both the HEMISPHERE and the CONTEXT considered; there was a
628 significant HEMISPHERE*CONTEXT*TIME interaction on a cluster of data points centered
629 over the Targets_q frequency ([16.4 Hz - 16.8 Hz]) and expanding from ROI_{Post_4} to ROI_{Post_5}
630 (cluster thresholded at .05; Figure 7.A), thus overlapping largely with the data points showing
631 the main effect of TIME. Interestingly, Fisher LSD post-hoc tests revealed that although
632 SSVEPs were comparable in both contexts at Stage_{Early}, whether considering the HEMI_{Contra-to-}
633 Target ($p = .503$) or the HEMI_{Ipsi-to-Target} ($p = .157$), they became different in both block types at
634 Stage_{Late}. In fact, the SSVEP amplitude in the HEMI_{Contra-to-Target} was surprisingly lower in MIBs
635 than in MCBs at this later stage ($p = .002$). Consistently, the SSVEP amplitude increased in the

636 HEMI_{Contra-to-Target} from Stage_{Early} to Stage_{Late} in MCBs ($p = .0008$) while it remained stable in
637 MIBs ($p = .879$). Such an increase from Stage_{Early} to Stage_{Late} did not occur in the HEMI_{Ipsi-to-}
638 Target, neither in MCBs ($p = .669$) nor in MIBs ($p = .072$), hence leading to comparable SSVEP
639 amplitudes in both contexts in the HEMI_{Ipsi-to-Target} at Stage_{Late} ($p = .988$).

640 Hence, the SSVEP data indicate that control processes recruited in anticipation of conflict
641 do not narrow or strengthen visual attention towards the goal-relevant stimulus location. On the
642 contrary, Targets_q SSVEP responses were smaller in MIBs compared to MCBs in the late stage
643 of the fixation period. Besides, Flanker-Ps_q SSVEP responses were globally higher in MIBs
644 than in MCBs. These results indicate a reduction of the focus of selective attention in MIBs.
645 Therefore, the higher accuracy of subjects in incongruent trials of MIBs cannot be accounted
646 for by an enhanced selectivity of visual attention.

647

648 *****

649 *Figure 7 about here*

650 *****

651

652 *RLP data*

653 Our cluster-based analysis revealed a significant main effect of the factor HEMISPHERE
654 on two clusters of data points (cluster thresholded at $p < .05$; Figure 8.A). A first cluster
655 extended from -350 to -200 ms with respect to movement onset and concerned the ROI_{Central_1-}
656 2 locations. Interestingly, in this time window, the RLP amplitude was higher (*i.e.*, more
657 negative) in the HEMI_{Ipsi-to-Resp} than in the HEMI_{Contra-to-Resp} ($p < .0001$; Figure 8.B). Then, a
658 later cluster expanded from -150 to -50 ms and concerned ROI_{Central_1-3}: in this time window,
659 the RLP amplitude was higher in the HEMI_{Contra-to-Resp} than in the HEMI_{Ipsi-to-Resp} ($p < .0001$,

660 respectively; Figure 8.B). Hence, on average, subjects initially showed a higher activity in the
661 motor cortex ipsilateral to the responding hand, compared to the contralateral one. The pattern
662 then reversed, with activity becoming stronger in the contralateral motor cortex as movement
663 execution drew nearer.

664

665

666 *****

667 *Figure 8 about here*

668 *****

669

670

671 Notably, the HEMISPHERE effect reported above on the first cluster (*i.e.*, from -350 to -
672 200 ms before movement onset) depended on the type of TRIAL the subjects encountered and
673 on the HAND they selected; there was a significant HEMISPHERE*HAND*TRIAL
674 interaction on a cluster of data points centered over the ROI_{Central_2} location and extending from
675 -320 to -150 ms, thus overlapping largely with the data points showing the HEMISPHERE
676 effect (cluster thresholded at $p < .05$; Figure 9.A).

677 In congruent trials, we observed a preponderant ipsilateral activity whether the subjects
678 responded with the left (*i.e.*, significant difference between HEMI_{Ipsi-to-Resp} and HEMI_{Contra-to-}
679 _{Resp}: $p = .012$) or the right hand ($p = .051$; Figure 9.B, C and D). Hence, action selection in the
680 flanker task involved an initial predominant increase in the activity of the ipsilateral motor
681 cortex, even in the absence of conflict.

682 Interestingly, in incongruent trials, this pattern of activity was observed for left (significant
683 difference between HEMI_{Ipsi-to-Resp} and HEMI_{Contra-to-Resp}: $p < .0001$) but not for right hand
684 responses ($p = .36$; Figure 9.B, C and D). Accordingly, left hand responses were associated with
685 a larger activity in the HEMI_{Ipsi-to-Resp} than right hand trials ($p = .0004$). Hence, in the presence
686 of conflict, ipsilateral activity was more pronounced in the dominant (left) motor cortex
687 (preceding left hand responses) than in the non-dominant (right) one (preceding right hand
688 responses). Notably, a similar effect was observed for the HEMI_{Contra-to-Resp}: contralateral
689 activity was larger in the dominant (left) motor cortex (preceding right hand responses) than in
690 the non-dominant (right) one (preceding left hand responses; $p = .019$). Altogether, these results
691 indicate that incongruent trials are associated with a stronger activation of the dominant motor
692 cortex compared to the non-dominant one, regardless of whether the response has to be
693 provided with the right (dominant) or the left (non-dominant) hand.

694

695

696 *****

697 *Figure 9 about here*

698 *****

699

700

701 Finally, our analysis also revealed a significant HEMISPHERE*TRIAL*CONTEXT
702 interaction on a cluster of data points extending from -300 to -190 ms and involving the
703 ROI_{Central_1-2} locations (cluster thresholded at $p < .05$; Figure 10.A).

704 We did not observe any effect of conflict expectation on motor activity in congruent trials.
705 RLPs were comparable in the MCB and MIB contexts, whether recorded in the HEMI_{Ipsi-to-Resp}
706 ($p = .17$; Figure 10.B, C and D) or the HEMI_{Contr-to-Resp} ($p = .09$). In contrast, we observed
707 significant differences in RLPs between the two block types for the HEMI_{Ipsi-to-Resp} in
708 incongruent trials. As such, ipsilateral activity was significantly larger in MIBs than in MCBs
709 ($p = .002$); such a context-dependent effect was not present for the HEMI_{Contr-to-Resp} ($p = .96$).

710 Hence, the RLP data suggest that conflict expectation does not reduce the impact of
711 incongruent stimuli on motor activity. On the contrary, activation of the ipsilateral motor cortex
712 became larger in the MIBs than in the MCBs following incongruent signals. Therefore, the
713 higher accuracy of subjects in incongruent trials of MIBs cannot be accounted for by a specific
714 reduction in the activation of inappropriate motor representations. Contrariwise, these cortical
715 representations were more active in MIBs than MCBs.

716 Altogether, our results confirm that subjects are better at resolving conflict when it is
717 expected in advance and that this enhancement is associated with a higher midfrontal theta
718 activity. Surprisingly, the SSVEP and RLP data point out that these changes occur in parallel
719 with a reduced filtering of information at the visual level and increased inappropriate activations
720 at the motor level. Hence, conflict expectation seems to recruit control processes that augment
721 the tolerance for inappropriate motor activations (rather than on processes that downregulate
722 their amplitude), allowing them to occur without leading to the selection of an incorrect
723 response. This mechanism might contribute to the enhancement of accuracy, but may restrain
724 decision speed.

725

726 *****

727 *Figure 10 about here*

728 *****

729

730 ***Methodological note***

731 Given the experimental design, congruent and incongruent trials could be either minority
732 (in MIB and MCB, respectively) or majority (in MCB and MIB, respectively). This means that
733 averages were computed on a varying amount of trials. To account for this possible bias when
734 analyzing the RLP data (not applicable for SSVEP and Δ SpectAmp data given the absence of
735 factor TRIAL for these dependent variables), additional analyses were run using an equalized
736 number of epochs across conditions (set based on the condition involving the smallest amount
737 of trials). Importantly, these analyses provided the same RLP results as those presented using
738 the full set of trials.

739 Another point of consideration for the RLP analysis concerns the time window used for
740 baseline correction (*i.e.*, -700 to -500 ms with respect to the response). As such, because the RT
741 varied between conditions (and between subjects), this time window could overlap with the last
742 second of the flickering period, either in part (*i.e.*, in the case of RTs longer than 500 ms), or in
743 total (*i.e.*, for RTs shorter than 500 ms). In other words, the baseline overlapped with the period
744 during which SSVEPs were induced. To control for this potential bias, we tested different time
745 windows for baseline correction (*i.e.*, -800 to -600 ms, -900 to -700 ms), getting back in time
746 with respect to the motor response, and thus increasing the fraction of the time window
747 overlapping with the flickering period. Again, we obtained the exact same results as in the main
748 analysis, indicating the robustness of the effects reported.

749

750

751

752 **DISCUSSION**

753 The primary goal of the present study was to investigate the impact of conflict expectation
754 on selective attention in the visual cortex and on action selection in the motor cortex. We
755 recorded SSVEPs and RLPs during an Eriksen Flanker task where conflict was either highly
756 predictable (MIBs) or very unlikely (MCBs). Besides, we also considered midfrontal theta
757 activity during the fixation period as a marker of cognitive control.

758 Midfrontal theta activity was higher in MIBs than in MCBs, indicating the engagement of
759 control processes recruited in anticipation of conflict: these are probably responsible for the fact
760 that subjects responded more accurately in incongruent trials when conflict was expected.
761 Notably, this enhanced accuracy in MIBs occurred at the cost of speed, as subjects became
762 slower to respond in congruent trials. Yet, surprisingly, visuomotor activity was less finely
763 tuned in MIBs. As such, target-related SSVEPs were smaller while peripheral flanker-related
764 SSVEPs were higher in MIBs than MCBs, and RLPs were larger in the ipsilateral motor cortex
765 during conflicting trials of MIBs. These findings suggest that conflict expectation recruits
766 cognitive control processes that augment the tolerance for inappropriate visuomotor activations,
767 allowing them to occur without leading to the selection of an incorrect action.

768 As expected, movement initiation was associated with a prominent activity in the motor
769 cortex contralateral to the responding hand. Indeed, contralateral RLPs became larger than
770 ipsilateral ones from -150 ms preceding movement onset, consistent with the literature (Nguyen
771 et al., 2014; Noorbaloochi et al., 2015). However, activity in the ipsilateral motor cortex was
772 surprisingly pronounced in our task, even in congruent trials. In fact, congruent trials were
773 associated with an initial boost of ipsilateral activity, which surpassed contralateral activity
774 from about -350 to -200 ms before movement onset, regardless of the context or of the
775 responding hand. Albeit not highlighted in the past, this effect seems also present in previous
776 studies using flanker tasks (Paasmra and Seiss, 2005; Klein et al., 2014). Why should the

777 ipsilateral (non-selected) motor cortex become so active soon after the imperative signal, even
778 in the absence of conflict? One possibility is that it has to do with the distribution of inhibitory
779 influences directed at motor representations during action preparation (Derosiere, 2018; Duque
780 et al., 2014, 2017). Indeed, these influences are predominantly directed at selected
781 representations (Quoilin and Derosiere, 2015; Vassiliadis et al., 2018) and only to a smaller
782 extent at non-selected ones. Given that EEG potentials result from the summation of excitatory
783 and inhibitory processes (Muthukumaraswamy et al., 2013), one may assume that the higher
784 activity initially observed in the ipsilateral motor cortex is due to the lower level of preparatory
785 inhibition directed at this (non-selected) area, compared to the selected, contralateral one.

786 Conflict expectation altered the strength of ipsilateral motor activity in incongruent trials
787 but not in congruent ones. Indeed, the RLP data revealed a comparable level of motor activity
788 for congruent trials, whether performed in MIBs or MCBs. Conversely, incongruent trials were
789 associated with a higher activity in the ipsilateral motor cortex in MIBs compared to MCBs.
790 This indicates that inappropriate motor activity following conflicting signals was larger when
791 conflict had been anticipated compared to when it occurred unexpectedly. Importantly, these
792 neural responses were obtained in trials where subjects turned out to select the correct action.
793 Hence, the (high) ipsilateral activity observed in MIBs must have remained nevertheless “below
794 threshold” given that it did not lead to the selection of an inappropriate response. This finding
795 suggests that conflict expectation is associated with an extension of the distance-to-threshold in
796 MIBs. Such an extension may be implemented by a rise in the selection threshold or by a
797 decrease in the level at which the motor cortex starts to accumulate neural activity (*i.e.*, the
798 starting point; Herz et al., 2017; Kim et al., 2017). In fact, several lines of evidence suggest that
799 conflict expectation could downregulate the starting point of neural accumulation. Indeed,
800 previous studies showed that the motor cortex exhibits a drop of baseline activity when task
801 requirements constrain subjects to focus on decision accuracy (Pastötter et al., 2011; Thura et

802 al., 2016) – *i.e.*, as when conflict occurrence is frequent. Along the same line, recent TMS
803 studies revealed that corticospinal excitability is globally suppressed when conflict is highly
804 expected compared to when it is unlikely (Klein et al., 2014; Duque et al., 2016). Most
805 noticeably, this global suppression has been evidenced at the time of the imperative signal,
806 consistent with a downregulation of the starting point of neural accumulation. Unfortunately,
807 the presence of such a shift cannot be detected in the current EEG dataset as pre-stimulus signals
808 are exploited to correct RLPs for baseline fluctuations, annihilating any putative differences in
809 baseline activity between the different conditions (Maess et al., 2016).

810 At the behavioral level, an enlarged distance-to-threshold is thought to produce a shift in
811 speed-accuracy tradeoff, favoring accuracy over speed, as revealed by studies using
812 computational modeling of behavioral data (Forstmann et al., 2010; Hauser et al., 2017; Thura
813 and Cisek, 2017). Accordingly, here (and in Burle et al., 2016), subjects were more accurate in
814 incongruent trials of MIBs than MCBs but showed longer RTs in easy, congruent trials. We
815 recognize that one would assume a shift in speed-accuracy tradeoff to induce a global reduction
816 of decision speed, altering RTs regardless of the trial type, while here (and in Burle et al., 2016),
817 the deceleration was only present in congruent trials. This may be due to the fact that subjects
818 had to respond under a fixed deadline. Given that RTs are long by default in incongruent trials
819 (*i.e.*, even in MCBs), the imposed time limit may have left little space for a further slow-down
820 in MIBs. Future studies should investigate the effect of conflict expectation on decision speed
821 in the absence of temporal constraints.

822 Incongruent trials were associated with a particularly low level of activity in the ipsilateral
823 motor cortex when conflict had not been expected in advance. As such, inappropriate motor
824 activity was less pronounced in MCBs than in MIBs, as explained above. Moreover, the
825 ipsilateral motor activity elicited by incongruent signals in MCBs was also less pronounced
826 than that recorded in the same context following congruent signals. Hence, when conflict

827 occurred unexpectedly, inappropriate motor activity was strongly restrained. One possibility is
828 that conflict detection in MCBs led to the recruitment of online control processes suppressing
829 inappropriate activations. Such an online inhibitory mechanism has been proposed to operate
830 during action reprogramming, as when sudden environmental changes call for the suppression
831 of habitual motor responses (Mars et al., 2009; Neubert et al., 2010), or when unexpected
832 obstacles require to abort initially-planned movement trajectories (Archambault et al., 2011).
833 Our results suggest that such process may also assist action selection in front of unexpected
834 conflict.

835 Interestingly, the efficiency of online control processes has been shown to depend on the
836 degree of visual attention directed at goal-relevant information (Reichenbach et al., 2014). Our
837 data are coherent with these previous findings. As such, we observed that the level of attention
838 directed towards the target location was stronger in MCBs than in MIBs, while attention to
839 goal-irrelevant locations was reduced in the former than in the latter context. A sharper
840 attentional focus in MCBs may have allowed subjects to limit the impact of incongruent
841 flankers on motor activity when they appeared unexpectedly. Such a control system may be
842 particularly prominent in contexts where conflict is rare, as it allows to limit the impact of
843 conflict when it occurs, without slowing down responses otherwise.

844 Hence, control strategies seem to be adapted to favor success in the most common type of
845 trials in a given context. A low distance-to-threshold combined with substantial online control
846 is the most efficient strategy in MCBs: it allows fast responses on most (congruent) trials while
847 ensuring a reasonable level of accuracy when conflict eventually occurs. In contrast, a proactive
848 control system extending the distance-to-threshold is the most efficient strategy in MIBs: it
849 allows accurate responses in most (incongruent) trials and the cost in terms of speed merely
850 concerns a minority of (congruent) trials.

851 Finally, another interesting finding concerns the involvement of the dominant motor cortex
852 in conflict resolution. In the presence of conflict, neural activity was higher in the left
853 (dominant) motor cortex than in the right (non-dominant) one, regardless of the responding
854 hand. This finding suggests that the left motor cortex contributes to a higher extent to the
855 resolution of visuomotor conflict than the right one. Consistently, control processes underlying
856 the execution of visually-guided movements are asymmetrically organized in the human brain
857 with a superiority of the left cerebral hemisphere (Bardi et al., 2012; Frey et al., 2008; Haaland
858 et al., 2004). Our findings indicate that the predominance of the left motor cortex goes beyond
859 motor control processes, and extends to motor decision-making. Moreover, because this effect
860 was observed in both MCBs and MIBs, the dominance of the left hemisphere seems to concern
861 conflict resolution regardless of the actual control strategy recruited to ensure appropriate
862 behavior.

863 In conclusion, the comparison of visuomotor activity in MCBs and MIBs suggests that
864 conflict resolution relies on distinct control strategies depending on the level of conflict
865 expectation. When most trials are conflicting, the distance-to-threshold may be generally
866 enlarged in a proactive way, allowing inappropriate visuomotor activity to occur without having
867 it cause incorrect responses, hence favoring accurate performance on most trials. Conversely,
868 when conflict is rare, the distance-to-threshold may be shorter, allowing fast responses on most
869 (congruent) trials; in this context, conflict resolution seems to rather rely on a sharp attentional
870 focus on the target with a low attention towards goal-irrelevant locations and on online
871 inhibition of inappropriate motor activity, preventing neural accumulation from reaching the
872 (low) selection threshold.

873

874

875

876 REFERENCES

- 877 Ardid S, Wang X-J (2013) A tweaking principle for executive control: neuronal circuit
878 mechanism for rule-based task switching and conflict resolution. *J Neurosci* 33:19504–
879 19517.
- 880 Bach M, Meigen T (1999) Do's and don'ts in Fourier analysis of steady-state potentials. *Doc
881 Ophthalmol* 99:69–82.
- 882 Bartoli E, Conner CR, Kadipasaoglu CM, Yellapantula S, Rollo MJ, Carter CS, Tandon N
883 (2017) Temporal Dynamics of Human Frontal and Cingulate Neural Activity During
884 Conflict and Cognitive Control. *Cereb Cortex* 1–15.
- 885 Bullmore ET, Suckling J, Overmeyer S, Rabe-Hesketh S, Taylor E, Brammer MJ (1999)
886 Global, voxel, and cluster tests, by theory and permutation, for a difference between two
887 groups of structural MR images of the brain. *IEEE Trans Med Imaging* 18:32–42.
- 888 Burle B, Spieser L, Roger C, Casini L, Hasbroucq T, Vidal F (2015) Spatial and temporal
889 resolutions of EEG: Is it really black and white? A scalp current density view. *Int J
890 Psychophysiol* 97:210–220.
- 891 Burle B, van den Wildenberg WPM, Spieser L, Ridderinkhof KR (2016) Preventing (impulsive)
892 errors: Electrophysiological evidence for online inhibitory control over incorrect
893 responses. *Psychophysiology* 53:1008–1019.
- 894 Castro L, Soto-Faraco S, Morís Fernández L, Ruzzoli M (2018) The breakdown of the Simon
895 effect in cross-modal contexts: EEG evidence. *Eur J Neurosci* 47:832–844.
- 896 Chabuda A, Durka P, Zygierek J (2018) High Frequency SSVEP-BCI With Hardware
897 Stimuli Control and Phase-Synchronized Comb Filter. *IEEE Trans Neural Syst Rehabil
898 Eng* 26:344–352.
- 899 Chen C, Muggleton N, Tzeng O, Hung D, Juan C (2009) Control of prepotent responses by the
900 superior medial frontal cortex. *Neuroimage* 44:537–545.
- 901 Clark K, Appelbaum LG, van den Berg B, Mitroff SR, Woldorff MG (2015) Improvement in
902 visual search with practice: mapping learning-related changes in neurocognitive stages of
903 processing. *J Neurosci* 35:5351–5359.
- 904 Cohen MX, Ridderinkhof KR (2013) EEG Source Reconstruction Reveals Frontal-Parietal
905 Dynamics of Spatial Conflict Processing Maurits NM, ed. *PLoS One* 8:e57293.
- 906 Correa Á, Rao A, Nobre AC (2009) Anticipating Conflict Facilitates Controlled Stimulus-
907 response Selection. *J Cogn Neurosci* 21:1461–1472.
- 908 Cottetereau BR, McKee SP, Norcia AM (2014) Dynamics and cortical distribution of neural
909 responses to 2D and 3D motion in human. *J Neurophysiol* 111:533–543.

- 910 Craddock M, Poliakoff E, El-deredy W, Klepousniotou E, Lloyd DM (2017) Pre-stimulus alpha
911 oscillations over somatosensory cortex predict tactile misperceptions. *Neuropsychologia*
912 96:9–18.
- 913 Delorme A, Makeig S (2004) EEGLAB: an open source toolbox for analysis of single-trial EEG
914 dynamics including independent component analysis. *J Neurosci Methods* 134:9–21.
- 915 Delorme A, Sejnowski T, Makeig S (2007) Enhanced detection of artifacts in EEG data using
916 higher-order statistics and independent component analysis. *Neuroimage* 34:1443–1449.
- 917 Derosiere G (2018) A dynamical system framework for theorizing preparatory inhibition. *J*
918 *Neurosci.* 38:3391–3393
- 919 Derosiere G, Billot M, Ward ET, Perrey S (2015a) Adaptations of motor neural structures'
920 activity to lapses in attention. *Cereb Cortex* 25:66–74.
- 921 Derosiere G, Farrugia N, Perrey S, Ward T, Torre K (2015b) Expectations induced by natural-
922 like temporal fluctuations are independent of attention decrement: Evidence from behavior
923 and early visual evoked potentials. *Neuroimage* 104:278–286.
- 924 Derosiere G, Vassiliadis P, Demaret S, Zénon A, Duque J (2017a) Learning stage-dependent
925 effect of M1 disruption on value-based motor decisions. *Neuroimage* 162:173–185.
- 926 Derosiere G, Zénon A, Alamia A, Duque J (2017b) Primary motor cortex contributes to the
927 implementation of implicit value-based rules during motor decisions. *Neuroimage*
928 146:1115–1127.
- 929 Di Russo F, Pitzalis S, Aprile T, Spitoni G, Patria F, Stella A, Spinelli D, Hillyard SA (2007)
930 Spatiotemporal analysis of the cortical sources of the steady-state visual evoked potential.
931 *Hum Brain Mapp* 28:323–334.
- 932 Diez PF, Mut VA, Avila Perona EM, Laciár Leber E (2011) Asynchronous BCI control using
933 high-frequency SSVEP. *J Neuroeng Rehabil* 8:39.
- 934 Duque J, Greenhouse I, Labruna L, Ivry RB (2017) Physiological Markers of Motor Inhibition
935 during Human Behavior. *Trends Neurosci* 40:219–236.
- 936 Duque J, Petitjean C, Swinnen SP (2016) Effect of aging on motor inhibition during action
937 preparation under sensory conflict. *Front Aging Neurosci* 8:1–14.
- 938 Eriksen BA, Eriksen CW (1974) Effects of noise letters upon the identification of a target letter
939 in a nonsearch task. *Percept Psychophys* 16:143–149.
- 940 Forstmann BU, Anwander A, Schäfer A, Neumann J, Brown S, Wagenmakers E-J, Bogacz R,
941 Turner R (2010) Cortico-striatal connections predict control over speed and accuracy in
942 perceptual decision making. *Proc Natl Acad Sci U S A* 107:15916–15920.

- 943 Frehlich M, Dominguez LG, Atluri S, Radhu N, Sun Y, Daskalakis ZJ, Farzan F (2016)
944 Unbiased cluster estimation of electrophysiological brain response. *J Neurosci Methods*
945 271:43–49.
- 946 Frey SH (2008) Tool use, communicative gesture and cerebral asymmetries in the modern
947 human brain. *Philos Trans R Soc B Biol Sci* 363:1951–1957.
- 948 Frigo M, Johnson SG (1998) FFTW: an adaptive software architecture for the FFT. In:
949 Proceedings of the 1998 IEEE International Conference on Acoustics, Speech and Signal
950 Processing, ICASSP '98 (Cat. No.98CH36181), pp 1381–1384. IEEE.
- 951 Groppe DM, Urbach TP, Kutas M (2011) Mass univariate analysis of event-related brain
952 potentials/fields I: a critical tutorial review. *Psychophysiology* 48:1711–1725.
- 953 Gruss LF, Wieser MJ, Schweinberger SR, Keil A (2012) Face-evoked steady-state visual
954 potentials: effects of presentation rate and face inversion. *Front Hum Neurosci* 6:316.
- 955 Gulbinaite R, Johnson A, de Jong R, Morey CC, van Rijn H (2014) Dissociable mechanisms
956 underlying individual differences in visual working memory capacity. *Neuroimage*
957 99:197–206.
- 958 Gulbinaite R, Van Viegen T, Wieling M, Cohen MX, Vanrullen R (2017) Individual alpha peak
959 frequency predicts 10 Hz flicker effects on selective attention. *J Neurosci*.
- 960 Hauser TU, Moutoussis M, Iannaccone R, Brem S, Walitza S, Drechsler R, Dayan P, Dolan RJ
961 (2017b) Increased decision thresholds enhance information gathering performance in
962 juvenile Obsessive-Compulsive Disorder (OCD) Gershman SJ, ed. *PLOS Comput Biol*
963 13:e1005440.
- 964 Heinrichs-Graham E, Wilson TW (2012) Presence of strong harmonics during visual
965 entrainment: a magnetoencephalography study. *Biol Psychol* 91:59–64.
- 966 Herz DM, Tan H, Brittain JS, Fischer P, Cheeran B, Green AL, Fitzgerald J, Aziz TZ, Ashkan
967 K, Little S, Foltynie T, Limousin P, Zrinzo L, Bogacz R, Brown P (2017) Distinct
968 mechanisms mediate speed-accuracy adjustments in cortico-subthalamic networks. *Elife*
969 6:1–25.
- 970 Keil A, Ihssen N, Heim S (2006) Early cortical facilitation for emotionally arousing targets
971 during the attentional blink. *BMC Biol* 4:23.
- 972 Keil A, Miskovic V, Gray MJ, Martinovic J (2013) Luminance, but not chromatic visual
973 pathways, mediate amplification of conditioned danger signals in human visual cortex. *Eur*
974 *J Neurosci* 38:3356–3362.
- 975 Kim D-W, Hwang H-J, Lim J-H, Lee Y-H, Jung K-Y, Im C-H (2011) Classification of selective
976 attention to auditory stimuli: Toward vision-free brain-computer interfacing. *J Neurosci*
977 *Methods* 197:180–185.

- 978 Kim YJ, Grabowecky M, Paller KA, Suzuki S (2010) Selective lateralization of steady state
979 visual evoked potentials at the second harmonic. *J Vis* 8:1002–1002.
- 980 Kim Y-J, Grabowecky M, Paller KA, Suzuki S (2011) Differential roles of frequency-following
981 and frequency-doubling visual responses revealed by evoked neural harmonics. *J Cogn*
982 *Neurosci* 23:1875–1886.
- 983 King JA, Korb FM, Egner T (2012) Priming of Control: Implicit Contextual Cuing of Top-
984 down Attentional Set. *J Neurosci* 32:8192–8200.
- 985 Klein PA, Duque J, Labruna L, Ivry RB (2016) Comparison of the two cerebral hemispheres in
986 inhibitory processes operative during movement preparation. *Neuroimage* 125:220–232.
- 987 Klein PA, Petitjean C, Olivier E, Duque J (2014) Top-down suppression of incompatible motor
988 activations during response selection under conflict. *Neuroimage* 86:138–149.
- 989 Lin H, Saunders B, Hutcherson CA, Inzlicht M (2018) Midfrontal theta and pupil dilation
990 parametrically track subjective conflict (but also surprise) during intertemporal choice.
991 *Neuroimage* 172:838–852.
- 992 Maess B, Schröger E, Widmann A (2016) High-pass filters and baseline correction in M/EEG
993 analysis. Commentary on: “How inappropriate high-pass filters can produce artefacts and
994 incorrect conclusions in ERP studies of language and cognition.” *J Neurosci Methods*
995 266:164–165.
- 996 Maris E, Oostenveld R (2007) Nonparametric statistical testing of EEG- and MEG-data. *J*
997 *Neurosci Methods* 164:177–190.
- 998 Mars RB, Klein MC, Neubert F-X, Olivier E, Buch ER, Boorman ED, Rushworth MFS (2009)
999 Short-Latency Influence of Medial Frontal Cortex on Primary Motor Cortex during Action
1000 Selection under Conflict. *J Neurosci* 29:6926–6931.
- 1001 McTeague LM, Gruss LF, Keil A (2015) Aversive learning shapes neuronal orientation tuning
1002 in human visual cortex. *Nat Commun* 6:7823.
- 1003 Melloni M, Sedeño L, Hesse E, García-Cordero I, Mikulan E, Plastino A, Marcotti A, López
1004 JD, Bustamante C, Lopera F, Pineda D, García AM, Manes F, Trujillo N, Ibáñez A (2015)
1005 Cortical dynamics and subcortical signatures of motor-language coupling in Parkinson’s
1006 disease. *Sci Rep* 5:11899.
- 1007 Michelet T, Duncan GH, Cisek P (2010) Response Competition in the Primary Motor Cortex:
1008 Corticospinal Excitability Reflects Response Replacement During Simple Decisions. *J*
1009 *Neurophysiol* 104:119–127.
- 1010 Moratti S, Keil A, Miller GA (2006) Fear but not awareness predicts enhanced sensory
1011 processing in fear conditioning. *Psychophysiology* 43:216–226.

- 1012 Mouraux A, Iannetti GD, Colon E, Nozaradan S, Legrain V, Plaghki L (2011) Nociceptive
1013 steady-state evoked potentials elicited by rapid periodic thermal stimulation of cutaneous
1014 nociceptors. *J Neurosci* 31:6079–6087.
- 1015 Müller MM, Andersen S, Trujillo NJ, Valdés-Sosa P, Malinowski P, Hillyard SA (2006)
1016 Feature-selective attention enhances color signals in early visual areas of the human brain.
1017 *Proc Natl Acad Sci U S A* 103:14250–14254.
- 1018 Murphy PR, Boonstra E, Nieuwenhuis S (2016) Global gain modulation generates time-
1019 dependent urgency during perceptual choice in humans. *Nat Commun* 7:1–14.
- 1020 Muthukumaraswamy SD, Carhart-Harris RL, Moran RJ, Brookes MJ, Williams TM, Errtizoe
1021 D, Sessa B, Papadopoulos A, Bolstridge M, Singh KD, Feilding A, Friston KJ, Nutt DJ
1022 (2013) Broadband cortical desynchronization underlies the human psychedelic state. *J
1023 Neurosci* 33:15171–15183.
- 1024 Neubert F-X, Mars RB, Buch ER, Olivier E, Rushworth MFS (2010) Cortical and subcortical
1025 interactions during action reprogramming and their related white matter pathways. *Proc
1026 Natl Acad Sci* 107:13240–13245.
- 1027 Nguyen VT, Breakspear M, Cunnington R (2014) Reciprocal Interactions of the SMA and
1028 Cingulate Cortex Sustain Premovement Activity for Voluntary Actions. *J Neurosci*
1029 34:16397–16407.
- 1030 Norcia AM, Appelbaum LG, Ales JM, Cottreau BR, Rossion B (2015) The steady-state visual
1031 evoked potential in vision research: A review. *J Vis* 15:4.
- 1032 Nozaradan S, Mouraux A, Cousineau M (2017) Frequency tagging to track the neural
1033 processing of contrast in fast, continuous sound sequences. *J Neurophysiol* 118:243–253.
- 1034 Nozaradan S, Peretz I, Missal M, Mouraux A (2011) Tagging the neuronal entrainment to beat
1035 and meter. *J Neurosci* 31:10234–10240.
- 1036 Nozaradan S, Peretz I, Mouraux A (2012) Steady-state evoked potentials as an index of
1037 multisensory temporal binding. *Neuroimage* 60:21–28.
- 1038 Oldfield RC (1971) The assessment and analysis of handedness: the Edinburgh inventory.
1039 *Neuropsychologia* 9:97–113.
- 1040 Pastötter B, Berchtold F, Bäuml KHT (2012) Oscillatory correlates of controlled speed-
1041 accuracy tradeoff in a response-conflict task. *Hum Brain Mapp* 33:1834–1849.
- 1042 Pernet CR, Latinus M, Nichols TE, Rousselet GA (2015) Cluster-based computational methods
1043 for mass univariate analyses of event-related brain potentials/fields: A simulation study. *J
1044 Neurosci Methods* 250:85–93.
- 1045 Poline J-B, Mazoyer BM (1993) Analysis of Individual Positron Emission Tomography
1046 Activation Maps by Detection of High Signal-to-Noise-Ratio Pixel Clusters. *J Cereb Blood
1047 Flow Metab* 13:425–437.

- 1048 Praamstra P, Seiss E (2005) The Neurophysiology of Response Competition: Motor Cortex
1049 Activation and Inhibition following Subliminal Response Priming. *J Cogn Neurosci*
1050 17:483–493.
- 1051 Quoilin C, Derosiere G (2015) Global and Specific Motor Inhibitory Mechanisms during
1052 Action Preparation. *J Neurosci* 35:16297–16299.
- 1053 Ridderinkhof KR (2002) Micro-and macro-adjustments of task set: activation and suppression
1054 in conflict tasks. *Psychol Res* 66:312–323.
- 1055 Rossion B, Prieto EA, Boremanse A, Kuefner D, Van Belle G (2012) A steady-state visual
1056 evoked potential approach to individual face perception: Effect of inversion, contrast-
1057 reversal and temporal dynamics. *Neuroimage* 63:1585–1600.
- 1058 Shen X, Finn ES, Scheinost D, Rosenberg MD, Chun MM, Papademetris X, Constable RT
1059 (2017) Using connectome-based predictive modeling to predict individual behavior from
1060 brain connectivity. *Nat Protoc* 12:506–518.
- 1061 Shioiri S, Honjyo H, Kashiwase Y, Matsumiya K, Kuriki I (2016) Visual attention spreads
1062 broadly but selects information locally. *Sci Rep* 6:35513.
- 1063 Spieser L, Van Den Wildenberg W, Hasbroucq T, Ridderinkhof KR, Burle B (2015)
1064 Controlling Your Impulses: Electrical Stimulation of the Human Supplementary Motor
1065 Complex Prevents Impulsive Errors. *J Neurosci* 35.
- 1066 Strack G, Kaufmann C, Kehrer S, Brandt S, Stürmer B (2013) Anticipatory regulation of action
1067 control in a simon task: behavioral, electrophysiological, and fMRI correlates. *Front
1068 Psychol* 4:47.
- 1069 Stuphorn V, Schall JD (2006) Executive control of countermanding saccades by the
1070 supplementary eye field. *Nat Neurosci* 9:925–931.
- 1071 Szűcs D, Soltész F, White S (2009) Motor conflict in Stroop tasks: Direct evidence from single-
1072 trial electro-myography and electro-encephalography. *Neuroimage* 47:1960–1973.
- 1073 Taylor PCJ, Nobre AC, Rushworth MFS (2007) Subsecond Changes in Top Down Control
1074 Exerted by Human Medial Frontal Cortex during Conflict and Action Selection: A
1075 Combined Transcranial Magnetic Stimulation Electroencephalography Study. *J Neurosci*
1076 27:11343–11353.
- 1077 Thura D, Cisek P (2014) Deliberation and commitment in the premotor and primary motor
1078 cortex during dynamic decision making. *Neuron* 81:1401–1416.
- 1079 Thura D, Cisek P (2016) Modulation of Premotor and Primary Motor Cortical Activity during
1080 Volitional Adjustments of Speed-Accuracy Trade-Offs. *J Neurosci* 36:938–956.
- 1081 Thura D, Cisek P (2017) The Basal Ganglia Do Not Select Reach Targets but Control the
1082 Urgency of Commitment. *Neuron* 95:1160–1170.e5.

- 1083 Töllner T, Wang Y, Makeig S, Müller HJ, Jung T-P, Gramann K (2017) Two Independent
1084 Frontal Midline Theta Oscillations during Conflict Detection and Adaptation in a Simon-
1085 Type Manual Reaching Task. *J Neurosci* 37:2504–2515.
- 1086 van Campen AD, Keuken MC, van den Wildenberg WPM, Ridderinkhof KR (2014) TMS over
1087 M1 Reveals Expression and Selective Suppression of Conflicting Action Impulses. *J Cogn*
1088 *Neurosci* 26:1–15.
- 1089 van Driel J, Swart JC, Egner T, Ridderinkhof KR, Cohen MX (2015) (No) time for control:
1090 Frontal theta dynamics reveal the cost of temporally guided conflict anticipation. *Cogn*
1091 *Affect Behav Neurosci* 15:787–807.
- 1092 Vassiliadis P, Grandjean J, Derosiere G, de Wilde Y, Quemener L, Duque, J (2018) Using a
1093 double-coil TMS protocol to assess preparatory inhibition bilaterally. *Front Neurosci*, 12,
1094 139.
- 1095 Verleger R, Kuniecki M, Möller F, Fritzmannova M, Siebner HR (2009) On how the motor
1096 cortices resolve an inter-hemispheric response conflict: an event-related EEG potential-
1097 guided TMS study of the flankers task. *Eur J Neurosci* 30:318–326.
- 1098 Vialatte F-B, Maurice M, Dauwels J, Cichocki A (2010) Steady-state visually evoked
1099 potentials: Focus on essential paradigms and future perspectives. *Prog Neurobiol* 90:418–
1100 438.
- 1101 Vidal F, Burle B, Spieser L, Carbonnell L, Meckler C, Casini L, Hasbroucq T (2015) Linking
1102 EEG signals, brain functions and mental operations: Advantages of the Laplacian
1103 transformation. *Int J Psychophysiol* 97:221–232.
- 1104 Vissers ME, Ridderinkhof KR, Cohen MX, Slagter HA (2018) Oscillatory Mechanisms of
1105 Response Conflict Elicited by Color and Motion Direction: An Individual Differences
1106 Approach. *J Cogn Neurosci* 30:468–481.
- 1107 Wang C-H, Yang C-T, Moreau D, Muggleton NG (2017) Motor expertise modulates neural
1108 oscillations and temporal dynamics of cognitive control. *Neuroimage* 158:260–270.
- 1109
- 1110
- 1111
- 1112
- 1113
- 1114

1115 **LEGENDS**

1116 **Figure 1: Task design.** **A.** Trial types. Subjects were asked to perform congruent (*upper panel*)
1117 and incongruent (*lower panel*) trials requiring left (*left panel*) or right (*right panel*) finger
1118 responses according to an imperative stimulus consisting of a central arrow (target) surrounded
1119 by two irrelevant arrows on each side (flankers). **B.** Time course of a typical trial. Each trial
1120 started with the presentation of five black squares remaining on the screen for 7000 ms (*top*
1121 *left*). Then, the imperative stimulus appeared (*top right*), indicating the required response (right
1122 key-press in current example). Once a response was provided (or after 700 ms), a mask appeared
1123 and remained on the screen for an interval of 1200 ms (*bottom right*). A feedback score was
1124 then displayed for 1500 ms depending on the subject RT and accuracy (*bottom left*). **C.** Block
1125 types. The experiment involved two block types including either a majority of congruent trials
1126 (MCB; *left*) or a majority of incongruent trials (MIB; *right*). Conflict expectation was highest
1127 in the latter block type. **D.** SSVEP procedure. In half of the blocks, the stimuli were slightly
1128 shifted to the left (*left panel*) whereas they were slightly shifted to the right in the other blocks
1129 (*right panel*). The target square (Targets_q) appeared on the left of the fixation cross in left-
1130 shifted stimuli and on the right of it in right-shifted stimuli; it was flickering at 16.6 Hz. The
1131 most central flanker square (Flanker- Cs_q) was flickering at 12.5 Hz; it was always the one
1132 located on the other side of the fixation point. The three more peripheral flanker squares
1133 (Flanker- Ps_q) were flickering at 14.2 Hz.

1134

1135 **Figure 2: EEG data processing steps.** **A.** Attention epochs - SSVEP. (1) For each subject,
1136 multiple Z-scored spectra were obtained (*i.e.*, in 4 conditions and 64 electrodes). Typical single-
1137 subject spectra are represented, showing three SSVEP peaks at 12.5, 14.2 and 16.6 Hz. (2) The
1138 spectra obtained at electrodes of a posterior region of interest (ROI_{Post}) were exploited to
1139 compute linear channel maps. (3) A cluster-based statistical analysis was applied on the maps

1140 to test for any significant effect of the factors of interest (*i.e.*, HEMISPHERE and CONTEXT)
1141 on the spectral amplitude among the frequency and scalp location dimensions. **B.** Selection
1142 epochs - RLP. (1) For each subject, multiple response-locked potentials were obtained (in
1143 $\mu\text{V}/\text{m}^2$; *i.e.*, in 16 conditions and 64 electrodes). Typical single-subject potentials are
1144 represented. (2) The potentials obtained at electrodes of a central ROI ($\text{ROI}_{\text{Central}}$) were
1145 exploited to compute channel maps. (3) A cluster-based statistical analysis was applied on the
1146 maps to test for any significant effect of the factors of interest (*e.g.*, TRIAL [congruent,
1147 incongruent], CONTEXT [MCB, MIB], *etc*) on the potential amplitude among the time and
1148 scalp location dimensions.

1149

1150 **Figure 3: Accuracy (upper traces; A-C) and RT (lower traces; D-F) data (mean \pm SE).**
1151 **A&D.** The HAND factor significantly impacted the accuracy and RT data. Green and blue
1152 colors represent data obtained for left and right hand responses, respectively. Both trial types
1153 and contexts are pooled together. **B&E.** The TRIAL factor had a significant influence on the
1154 accuracy and RT data. Both hands and contexts are pooled together. **C&F.** The
1155 TRIAL*CONTEXT interaction was significant. Both hands are pooled together. *: Significant
1156 difference at $p < .05$.

1157

1158 **Figure 4: Effect of conflict expectation on midfrontal theta activity.** **A.** The cluster-based
1159 statistical analysis revealed that $\Delta\text{SpectPower}$, a marker of theta activity due to conflict
1160 expectation, was significantly different from 0 for a cluster of data points in the theta range. **B.**
1161 Grand-average TF maps were obtained for the Fpz (top), Fz (middle) and Cz (bottom)
1162 electrodes. For illustrative purposes, maps were resampled by multiplying temporal and
1163 frequency resolutions by a factor of 10. The rectangle delineated by black dotted lines highlights
1164 the significant cluster on each map: note the significantly higher $\Delta\text{SpectPower}$ for the

1165 midfrontal Fz electrode specifically (absence of effect for the two other electrodes). **C.** Grand-
1166 average topography were obtained using the time-frequency boundaries of the detected cluster
1167 to extract the values at each electrode: [+4700 ms +5400 ms] / [6 8 Hz]. **D.** Post-hoc results
1168 show the larger Δ SpectPower for Fz compared to Fpz and Cz. Time-frequency boundaries used
1169 to extract the cluster-level average values in each subject are the same as in C. Bar graphs
1170 represent group-level mean \pm SE. *: Significant difference at $p < .05$.

1171

1172 **Figure 5: Effect of the factor HEMISPHERE on SSVEPs.** **A.** The cluster-based statistical
1173 analysis revealed a significant main effect of HEMISPHERE on two clusters of data points,
1174 highlighted in red. **B.** Effect of HEMISPHERE at the Flanker-C_{sq} frequency. *Top:* Grand-
1175 average channel maps as obtained for HEMI_{Contra-to-Target} (left) and HEMI_{Ipsi-to-Target} (right;
1176 ipsilateral and contralateral to the Flanker-C_{sq}, respectively). The ROI_{Post} locations (2-5)
1177 showing a significant HEMISPHERE effect are comprised in the rectangles delineated by the
1178 black dotted lines. *Bottom left:* Grand-average frequency spectra (all electrodes composing the
1179 cluster pooled together) as obtained for the HEMI_{Contra-to-Target} (solid line) and HEMI_{Ipsi-to-Target}
1180 (dashed line). The gray rectangle highlights the frequency window of statistical significance. *:
1181 Significant difference at $p < .05$. *Bottom right:* Grand-average topographies at 12.5 Hz for left-
1182 and right-shifted stimuli (left and right topographies, respectively). The electrodes composing
1183 the detected cluster are highlighted by small black stars. **C.** Same as B. for the Targets_{sq}
1184 frequency.

1185

1186 **Figure 6: Effect of the factor CONTEXT on SSVEPs.** **A.** The cluster-based statistical
1187 analysis revealed a significant main effect of CONTEXT on two clusters of data points,
1188 highlighted in red. **B.** SSVEP amplitude in MCB (orange) and MIB (red) blocks. *Top left:*
1189 Grand-average channel maps as obtained for MCBs and MIBs. The ROI_{Post} locations (1-3)

1190 showing a significant effect of the factor CONTEXT at the Flanker-P_{Sq} frequency are comprised
1191 in the rectangles delineated by the black dotted lines. *Top right:* Grand-average frequency
1192 spectra (all electrodes composing the cluster pooled together) as obtained for the MCBs
1193 (orange) and MIBs (red). Note the higher Flanker-P_{Sq}-related SSVEPs in MIBs compared to
1194 MCBs. The gray rectangle highlights the frequency window of statistical significance. *:
1195 Significant difference at $p < .05$. *Bottom:* Grand-average topographies at 14.2 Hz for left- and
1196 right-shifted stimuli (left and right topographies, respectively). The electrodes composing the
1197 detected cluster are highlighted by small black stars.

1198

1199 **Figure 7: Effect of the HEMISPHERE*CONTEXT*TIME interaction on SSVEPs. A.** The
1200 cluster-based statistical analysis revealed a significant HEMISPHERE*CONTEXT*TIME
1201 interaction on a cluster of data points, highlighted in red. **B.** At Stage_{Early}. *Top:* Grand-average
1202 channel maps as obtained for HEMI_{Contra-to-Target} (left) and HEMI_{Ipsi-to-Target} (right), in MCBs
1203 (top) and MIBs (bottom). The ROI_{Post} locations (4-5) showing a significant
1204 HEMISPHERE*CONTEXT*TIME interaction are comprised in the rectangles delineated by
1205 the black dotted lines. *Bottom left:* Grand-average frequency spectra as obtained for the
1206 HEMI_{Contra-to-Target} (solid line) and HEMI_{Ipsi-to-Target} (dashed line), in MCBs (orange) and MIBs
1207 (red). The frequency spectra measured at the electrodes composing the detected cluster were
1208 averaged together. The gray rectangle highlights the frequency window of statistical
1209 significance. *: Significant difference at $p < .05$. *Bottom right:* Grand-average topographies at
1210 16.6 Hz for left- and right-shifted stimuli (left and right topographies, respectively). The
1211 electrodes composing the detected cluster are highlighted by small black stars. **C.** Same as *B*.
1212 for the Stage_{Late}. *: Significant difference at $p < .05$.

1213

1214 **Figure 8: Effect of the factor HEMISPHERE on RLPs.** **A.** The cluster-based statistical
1215 analysis revealed a significant main effect of the HEMISPHERE factor on two clusters of data
1216 points, highlighted in red. **B. Top panel:** Grand-average channel maps as obtained for
1217 HEMI_{Contra-to-Resp} (left) and HEMI_{Ipsi-to-Resp} (right). The ROI_{Central} locations showing a significant
1218 effect of HEMISPHERE are comprised in the rectangles delineated by the black dotted lines.
1219 *Bottom-left panel:* Grand-average RLP waveforms as obtained for the HEMI_{Contra-to-Resp} (solid
1220 line) and HEMI_{Ipsi-to-Resp} (dashed line). The RLPs measured at the electrodes composing the two
1221 detected clusters were averaged separately; that is, ROI_{Central_1} and ROI_{Central_2} were exploited
1222 to compute the left segment of the RLP (from - 500 ms to -150 ms) while the averaging for the
1223 right segment also involved ROI_{Central_3} (from -150 to -50 ms). The two gray rectangles highlight
1224 the time windows of statistical significance. *: Significant difference at $p < .05$. *Bottom-right*
1225 *panel:* Grand-average topographies at -250 ms and -100 ms (left and right topographies,
1226 respectively) for left hand responses. The electrodes composing each detected cluster are
1227 highlighted by small black stars.

1228

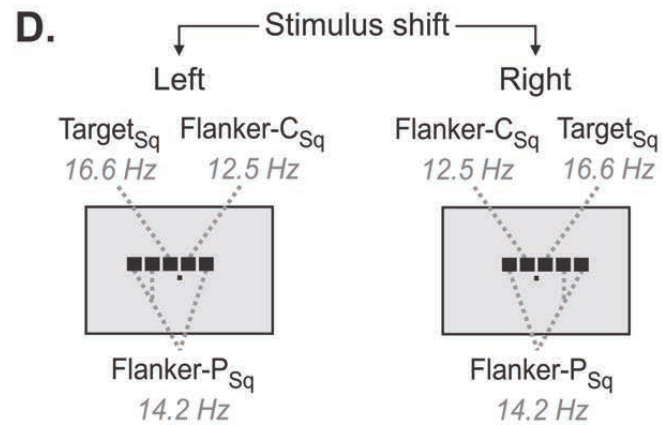
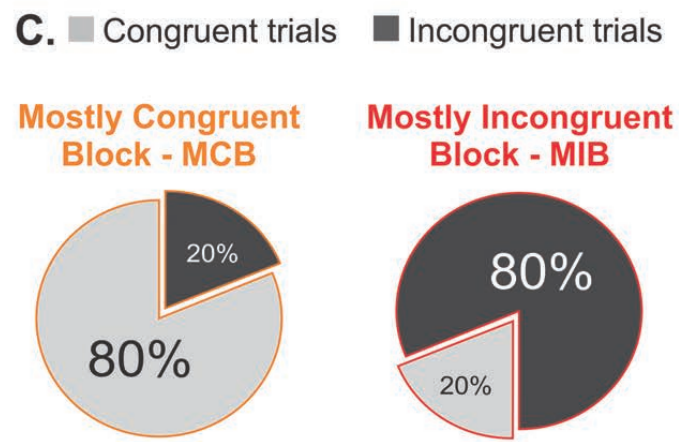
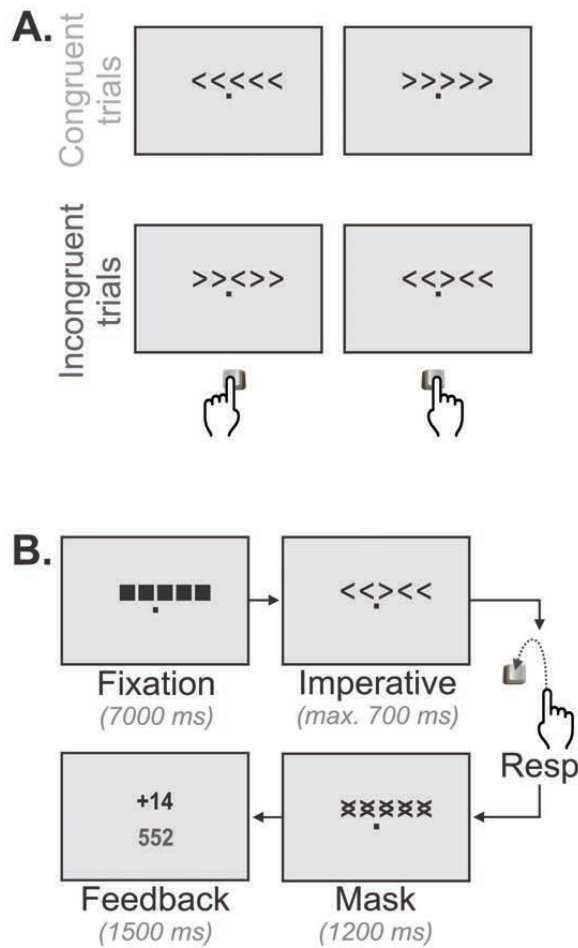
1229 **Figure 9: Effect of the HEMISPHERE*HAND*TRIAL interaction on RLPs.** **A.** The
1230 cluster-based statistical analysis revealed a significant main effect of the
1231 HEMISPHERE*HAND*TRIAL interaction on a cluster of data points, highlighted in red. **B.**
1232 *Left panel:* Grand-average channel maps as obtained for congruent trials, for left (top row) and
1233 right (bottom row) hand responses, in HEMI_{Contra-to-Resp} (left column) and HEMI_{Ipsi-to-Resp} (right
1234 column). The ROI_{Central} location showing a significant HEMISPHERE*HAND*TRIAL
1235 interaction is comprised in the rectangles delineated by the black dotted lines. *Right panel:*
1236 Same as *B. Left panel* for incongruent trials. **C. Left panel:** Grand-average RLP waveforms as
1237 obtained for congruent (left column) and incongruent (right column) trials, for left (top row;
1238 green) and right (bottom row; blue) responses, in the HEMI_{Contra-to-Resp} (solid lines) and

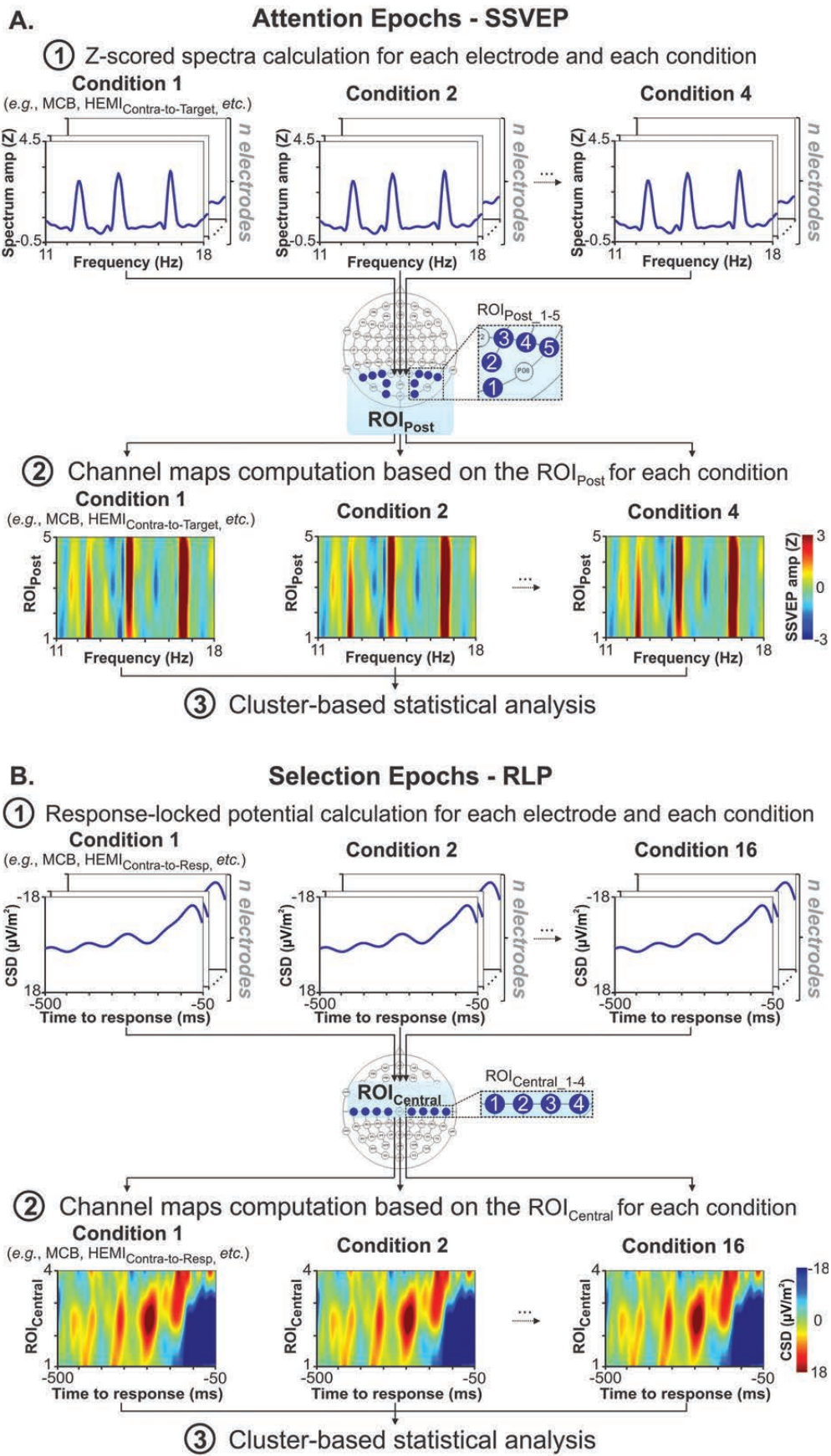
1239 HEMI_{Ipsi-to-Resp} (dashed lines). The RLP waveform measured at the electrode composing the
1240 detected cluster was extracted for each condition. The gray rectangle highlights the time
1241 window of statistical significance. *: Significant difference at $p < .05$. *Right panel*: The same
1242 RLP waveforms as the ones represented in *C. Left panel* were exploited to highlight the
1243 significant differences in RLP amplitude for left and right responses in incongruent trials. RLPs
1244 obtained in the HEMI_{Contra-to-Resp} and HEMI_{Ipsi-to-Resp} are represented at top and bottom rows,
1245 respectively. **D.** Grand-average topographies for congruent (left; obtained at - 250 ms) and
1246 incongruent (right; at - 200 ms) trials. For each trial type, topographies for both hand responses
1247 are represented. The electrode composing the detected cluster is highlighted by small black
1248 stars.

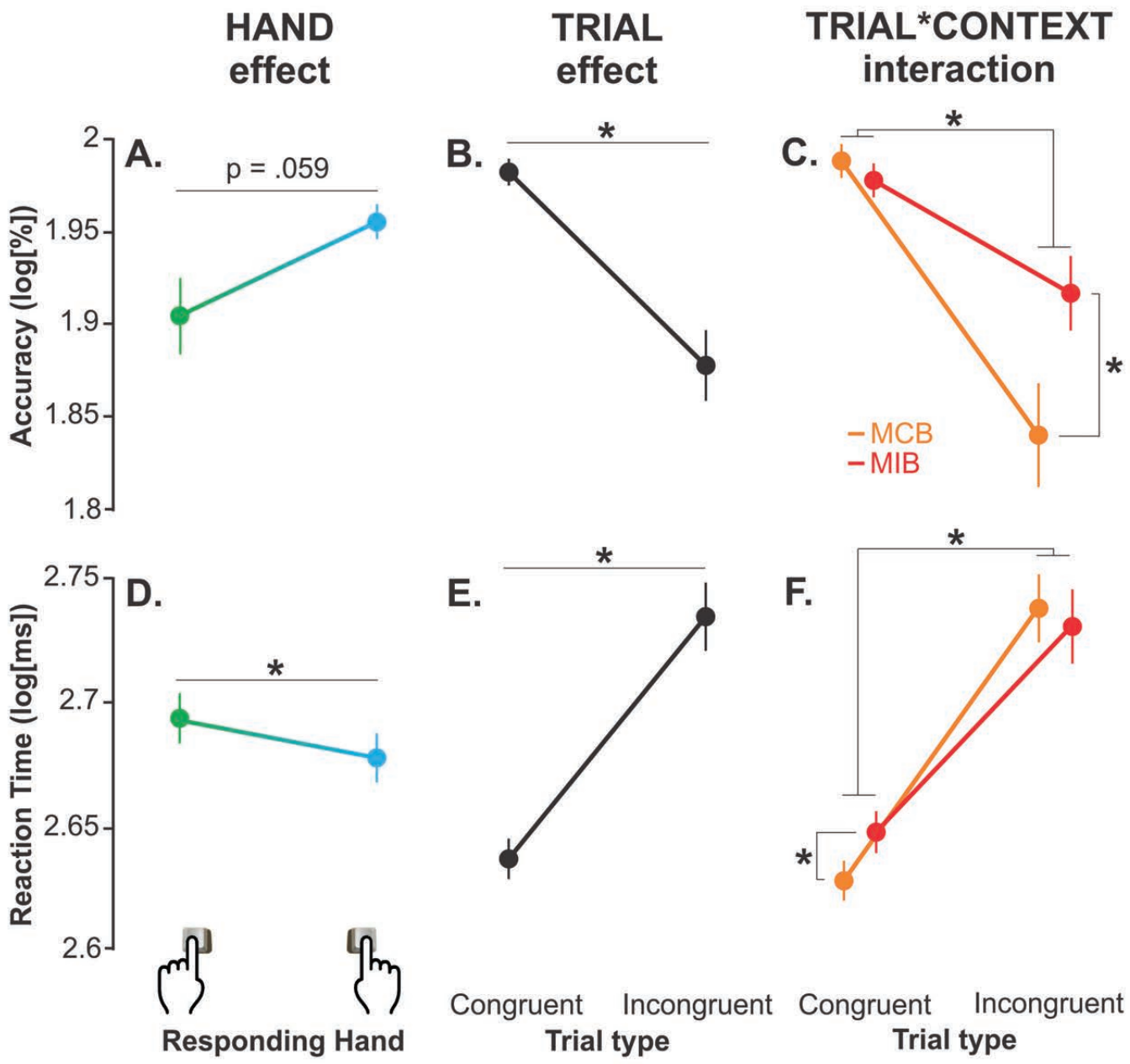
1249

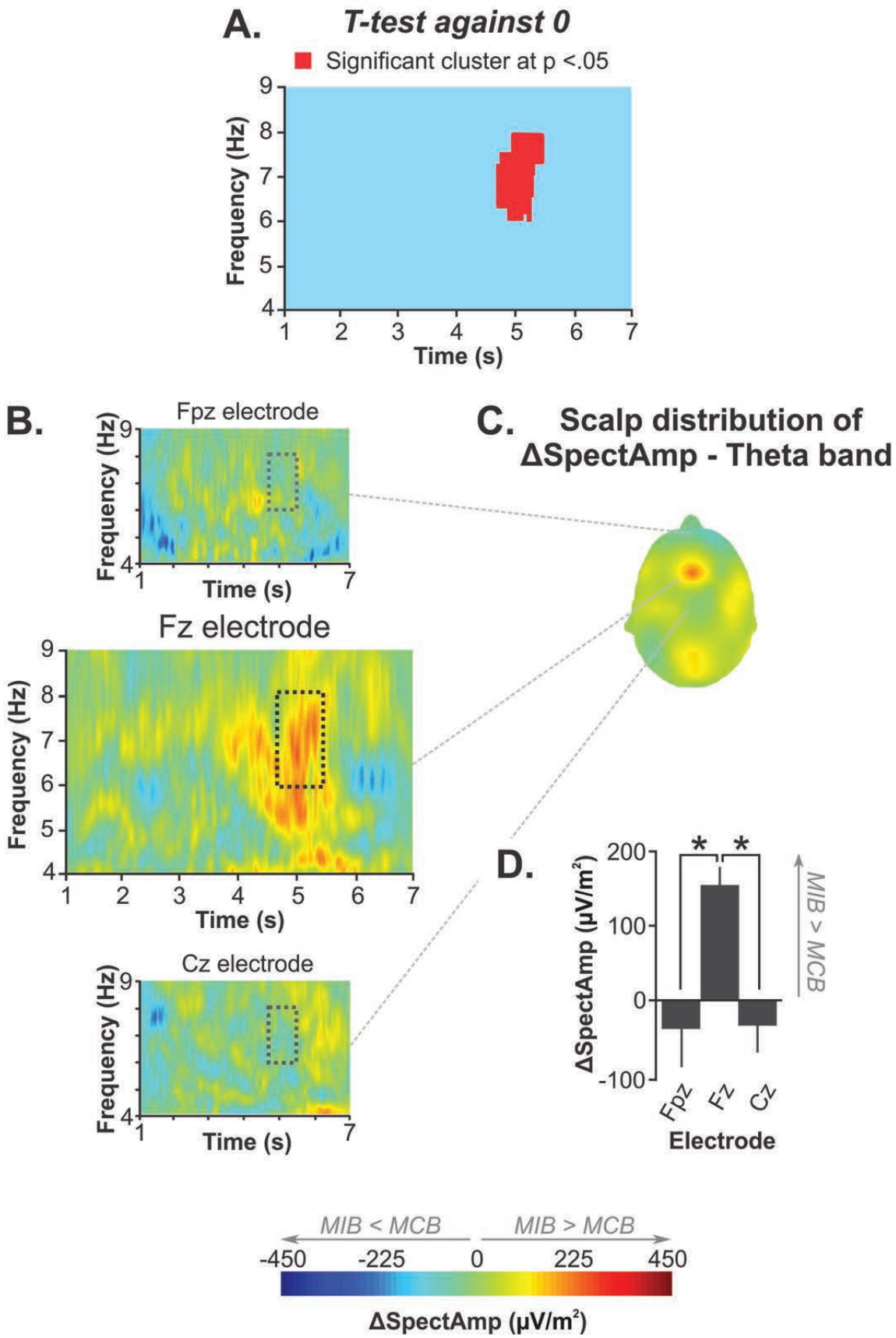
1250 **Figure 10: Effect of the HEMISPHERE*TRIAL*CONTEXT interaction on RLPs. A.** The
1251 cluster-based statistical analysis revealed a significant main effect of the
1252 HEMISPHERE*TRIAL*CONTEXT interaction on a cluster of data points, highlighted in red.
1253 **B. Left panel:** Grand-average channel maps as obtained for congruent trials, for MCB (top row)
1254 and MIB (bottom row) contexts, in HEMI_{Contra-to-Resp} (left column) and HEMI_{Ipsi-to-Resp} (right
1255 column). The ROI_{Central} location showing a significant HEMISPHERE*TRIAL*CONTEXT
1256 interaction is comprised in the rectangles delineated by the black dotted lines. **Right panel:**
1257 Same as *B. Left panel* for incongruent trials. **C. Left panel:** Grand-average RLP waveforms as
1258 obtained for congruent (left column) and incongruent (right column) trials, for MCB (top row;
1259 orange) and MIB (bottom row; red) contexts, in the HEMI_{Contra-to-Resp} (solid lines) and HEMI_{Ipsi-}
1260 _{to-Resp} (dashed lines). The RLP waveforms measured at the electrodes composing the detected
1261 cluster were averaged together for each condition. The gray rectangle highlights the time
1262 window of statistical significance. *: Significant difference at $p < .05$. *Right panel*: The same
1263 RLP waveforms as the ones represented in *C. Left panel* were exploited to highlight the

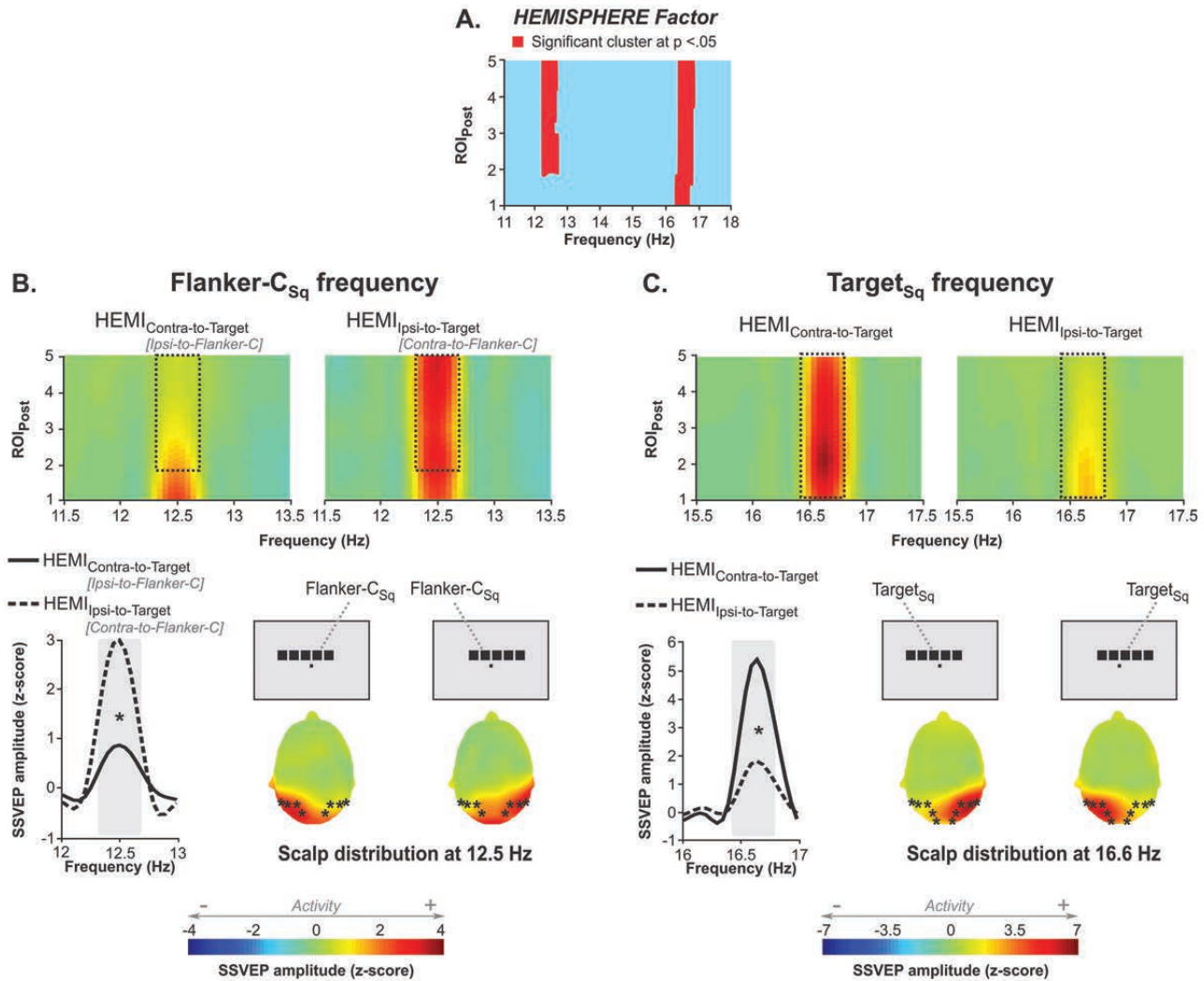
1264 significant differences in RLP amplitude in the HEMI_{Ipsi-to-Resp} between MCB and MIB contexts
1265 in incongruent trials. RLPs obtained in the HEMI_{Contra-to-Resp} and HEMI_{Ipsi-to-Resp} are represented
1266 at top and bottom rows, respectively. **D.** Grand-average topographies obtained at -230 ms for
1267 congruent (left) and incongruent (right) trials. For each trial type, topographies for both hand
1268 responses and both contexts are represented. The electrodes composing the detected cluster are
1269 highlighted by small black stars.

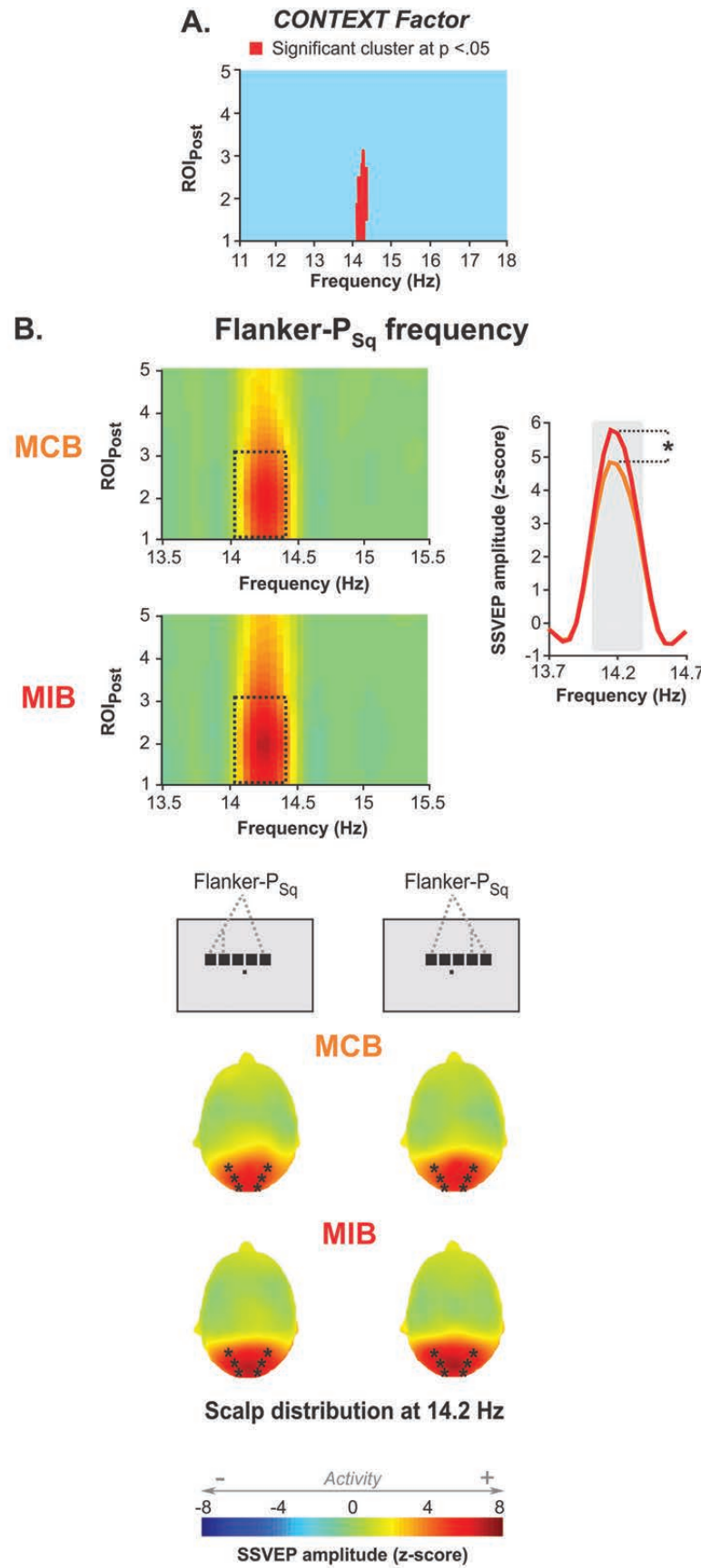


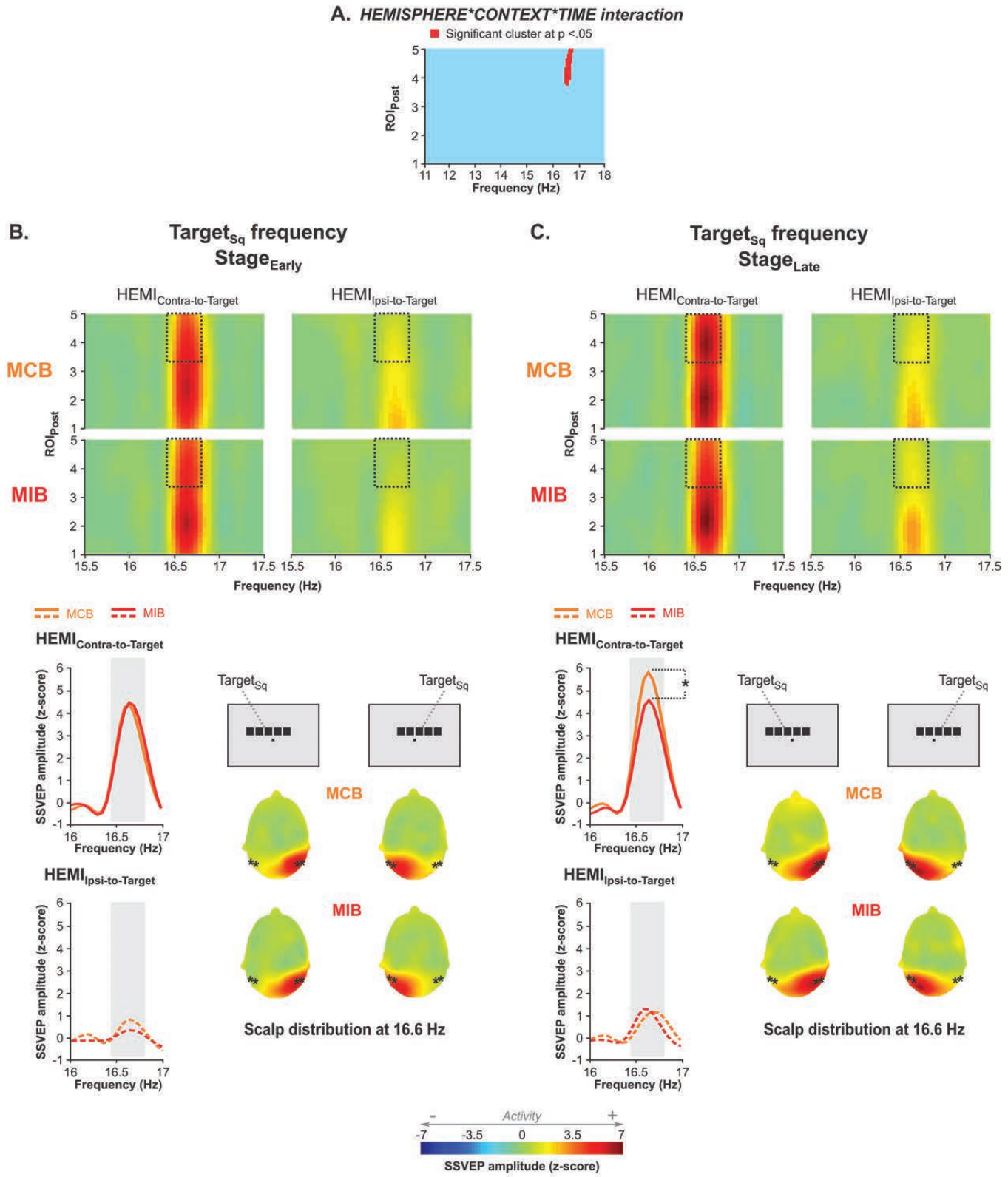


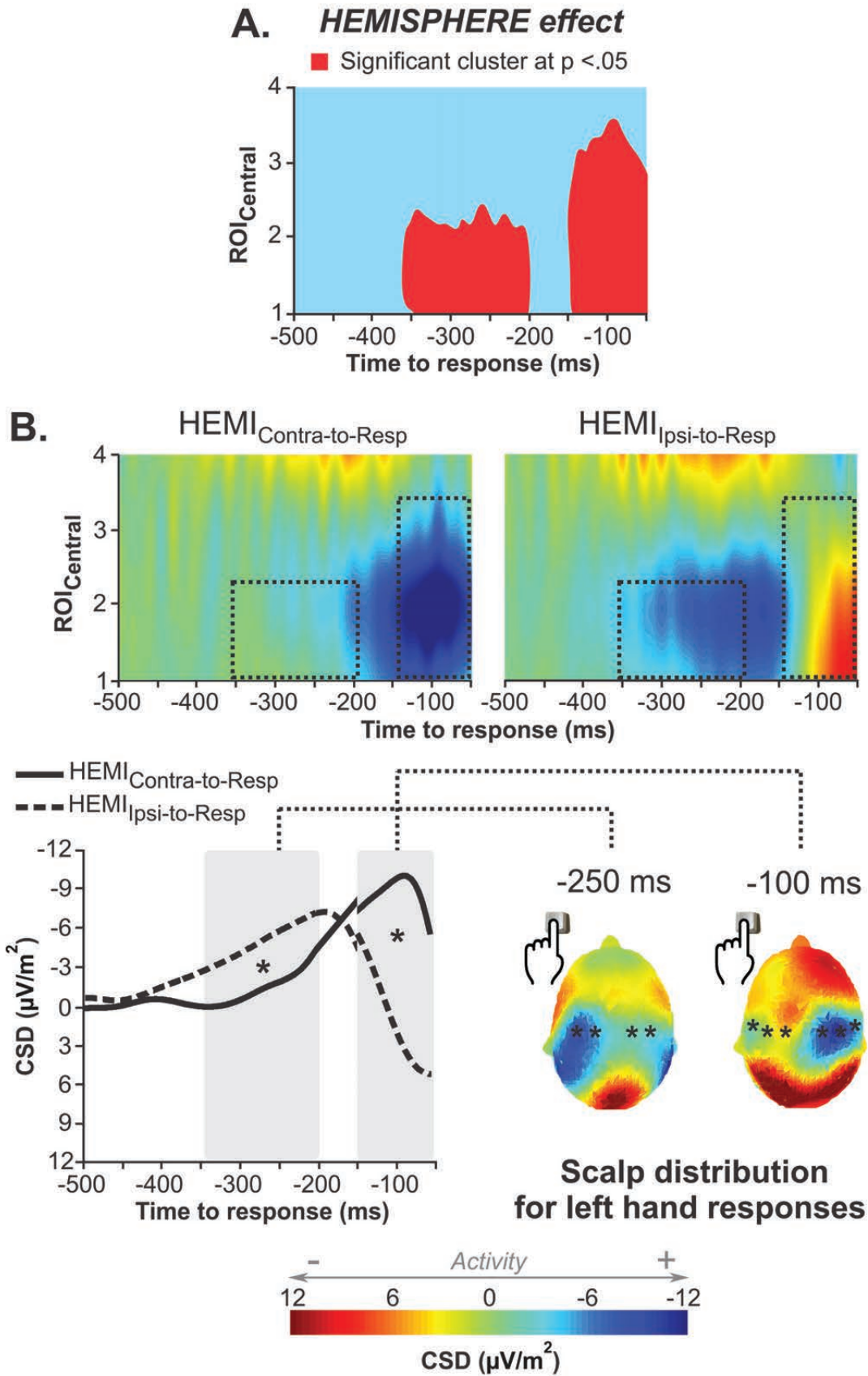


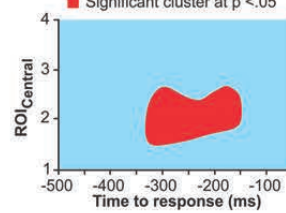
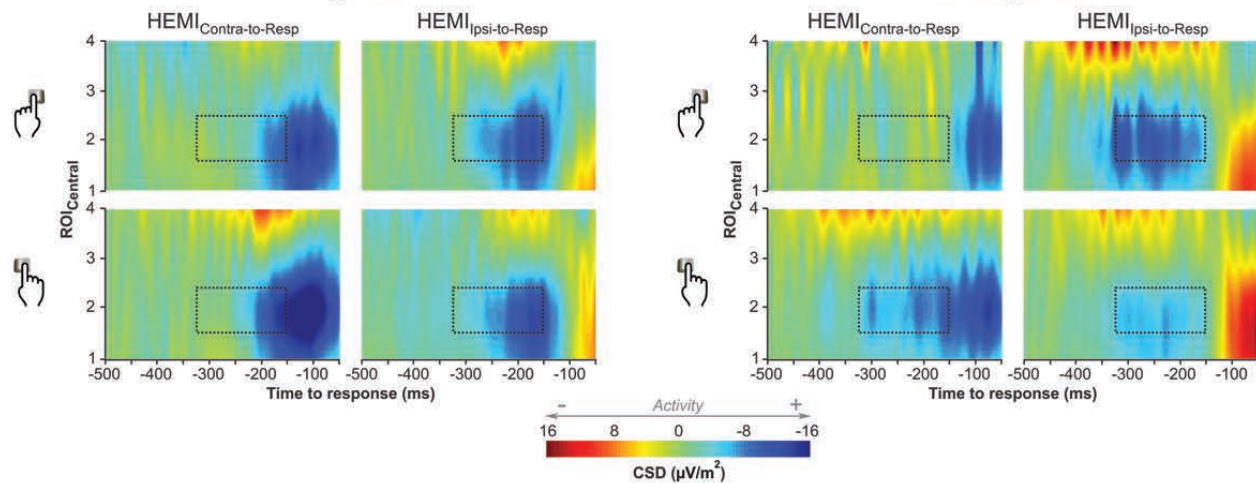
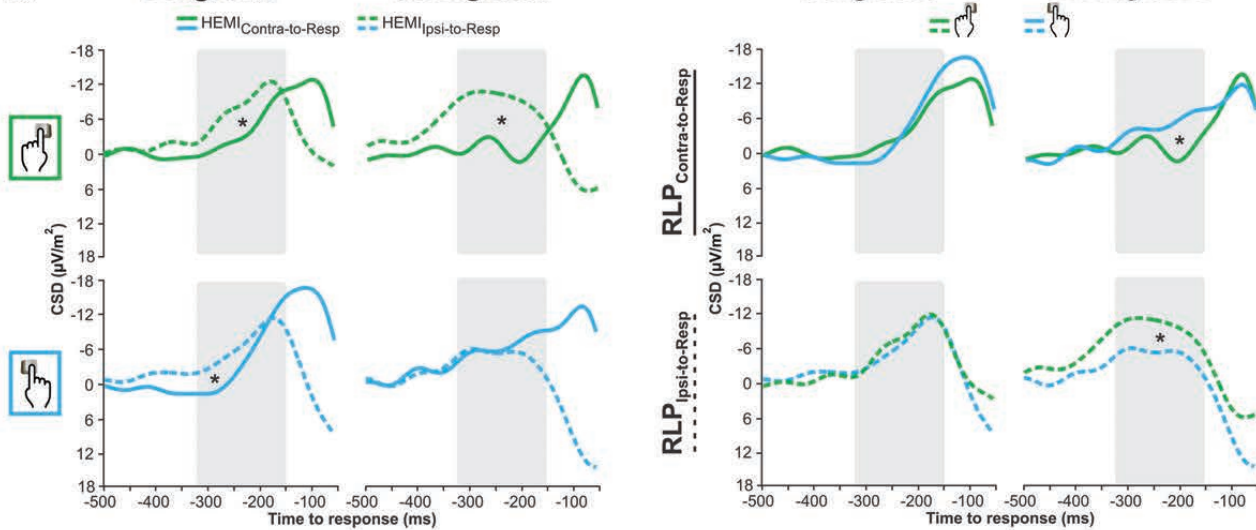










A. HEMISPHERE*HAND*TRIAL interaction■ Significant cluster at $p < .05$ **B.****Congruent****Incongruent****C.****Congruent****Incongruent****D. Congruent**

-250 ms

Incongruent

-200 ms

Scalp distribution